NASA TECHNICAL NOTE

NASA TN D-6591

ION-THRUSTER PROPELLANT UTILIZATION

by Harold R. Kaufman

Lewis Research Center
Cleveland, Ohio 44135

NATIONAL AERONAUTICS AND SPACE ADMINISTRATION • WASHINGTON, D. C. • DECEMBER 1971

1. Report No.	2. Government Accession No.	3. Recipient's Catalog No.
NASA TN D-6591		

4. Title and Subtitle	5. Report Date
ION-THRUSTER PROPELLANT UTILIZATION	December 1971
	6. Performing Organization Code

7. Author(s)	8. Performing Organization Report No.
Harold R. Kaufman	E-6219
	10. Work Unit No.
9. Performing Organization Name and Address	113-26
Lewis Research Center National Aeronautics and Space Administration Cleveland, Ohio 44135	11. Contract or Grant No.
12. Sponsoring Agency Name and Address	13. Type of Report and Period Covered
National Aeronautics and Space Administration Washington, D.C. 20546	Technical Note
	14. Sponsoring Agency Code

15. Supplementary Notes

16. Abstract

The overall thruster efficiency is proportional to the propellant utilization, with propellant utilization defined (for singly ionized atoms) as the fraction of total propellant flow that is ionized and accelerated to form the ion beam. An improvement in propellant utilization can thus be translated directly into improved thruster performance. The subject of this investigation is the evaluation and understanding of maximum propellant utilization, with mercury used as the propellant. The primary-electron region in the ion chamber of a bombardment thruster is analyzed at maximum utilization. The results of this analysis, as well as experimental data from a range of ion-chamber configurations, show a nearly constant loss rate for unionized propellant at maximum utilization over a wide range of total propellant flow rate. The discharge loss level of 1000 eV/ion was used as a definition of maximum utilization, but the exact level of this definition has no effect on the qualitative results and little effect on the quantitative results. There are obvious design applications for the results of this investigation, but the results are particularly significant whenever efficient throttled operation is required.

17. Key Words (Suggested by Author(s))	18. Distribution Statement
Electric propulsion Ion source	Unclassified - unlimited

19. Security Classif. (of this report)	20. Security Classif. (of this page)	21. No. of Pages	22. Price*
Unclassified	Unclassified	57	$3.00

* For sale by the National Technical Information Service, Springfield, Virginia 22151

ION-THRUSTER PROPELLANT UTILIZATION*

by Harold R. Kaufman

Lewis Research Center

SUMMARY

The overall thruster efficiency is proportional to the propellant utilization, with propellant utilization defined (for singly ionized atoms) as the fraction of total propellant flow that is ionized and accelerated to form the ion beam. An improvement in propellant utilization can thus be translated directly into improved thruster performance. The subject of this investigation is the evaluation and understanding of maximum propellant utilization, with mercury used as the propellant. The primary-electron region in the ion chamber of a bombardment thruster is analyzed at maximum utilization. The results of this analysis, as well as experimental data from a range of ion-chamber configurations, show a nearly constant loss for un-ionized propellant at maximum utilization over a wide range of total propellant flow rate. The discharge loss level of 1000 eV per ion was used as a definition of maximum utilization, but the exact level of this definition has no effect on the qualitative results and little effect on the quantitative results. There are obvious design applications for the results of this investigation, but the results are particularly significant whenever efficient throttled operation is required.

INTRODUCTION

The mercury electron-bombardment ion thruster was introduced in 1960 (refs. 1 to 2). (Although ref. 1 was published in Nov. 1960, ref. 2 was actually written first.) Bombardment by electrons had, of course, been used to produce ions prior to 1960. The need in electric propulsion was for a copious source of ions, but with a low enough current density to permit the integration of the source with long-lived accelerators operating at exhaust velocities of interest for propulsion applications. The earlier electron-bombardment ion sources either produced too few ions to be of interest or

*The material presented in this report was submitted as a thesis in partial fulfillment of the requirements for the degree Doctor of Philosophy, Colorado State University, Fort Collins, Colorado, June 1971.

produced too high an ion current density to be used with practical electric-propulsion accelerators (refs. 3 to 10). In addition, most of the earlier sources were developed for specific applications, so that the source itself was often of secondary interest and inadequate information was given for evaluation in other applications.

The performance of the early electron-bombardment thrusters showed advantages over the performance of other ion thrusters of that period (ref. 11). These advantages led to a substantial research program on the bombardment type of thruster (refs. 12 to 141). Propellants other than mercury have been investigated, but only cesium appears to be a practical alternative to mercury (refs. 142 to 156). Because the primary interest in space propulsion is for mercury propellant, and because there are fundamental differences in operation with cesium, the past work with mercury will be emphasized in the following historical review.

Historical Development

The most characteristic part of an electron-bombardment thruster is the ion chamber, which started as a simple cylinder having a nearly uniform magnetic field roughly parallel to its axis. Most of the later improvements have been associated with the magnetic-field shape. First, the field windings were designed to give a decreasing magnetic field in the downstream direction (ref. 12). This shape is usually referred to as a divergent field. The strength of the optimum magnetic field was found to vary inversely with thruster diameter, with the optimum in the range 1×10^{-3} to 5×10^{-3} tesla (10 to 50 G) for a 10-centimeter-diameter thruster. An increase in magnetic-field strength was found to decrease ion-chamber losses at low values of field strength (ref. 12). The practical limit for magnetic-field strength was obtained when a further increase in field strength yielded a negligible decrease - or even an increase - in ion-chamber losses. More detailed investigations conducted later showed that ion-chamber noise increased with magnetic-field strength at high field-strength values (refs. 51 and 66), which indicated that collective or wave interactions were limiting electron containment at these higher field strengths. Iron pole pieces were added to increase the divergence of field lines in more recent designs (refs. 50 and 80). These pole pieces were originally incorporated as part of permanent-magnet designs (refs. 26 and 50) but have since become important tools for shaping the magnetic field. These pole pieces are therefore also employed on more recent thrusters that use electromagnets (refs. 95, 112, 119, and 141).

The foregoing constitutes the main line of magnetic-field configuration development, but some other concepts deserve mention. An Ioffe quadrupole magnetic field was adapted from fusion research (ref. 103) but gave no improvement in performance despite a decrease in plasma noise. The multipole "picket-fence" concept of plasma contain-

ment from fusion research has been employed in a cesium thruster (ref. 148) with a substantial improvement in performance. This last magnetic-field configuration has also been used with mercury propellant but gave no significant improvement over other configurations included in the same investigation (ref. 113).

A less important, but still significant aspect of ion-chamber design is that of propellant introduction. The first approach was to introduce the propellant at one end of the ion chamber and to let it flow through to the accelerator system on the other end. An investigation of various propellant introduction locations then showed that introduction at the downstream end of the chamber (reverse feed) gave a substantial reduction in losses (ref. 37). The effects of magnetic-field shape and propellant introduction are interrelated, though, so that the amount of improvement possible by changing the propellant introduction mode is less for the more recent divergent-field configurations. In fact, for the SERT II configuration, little change was noted with introduction mode except for introduction near the cathode (ref. 80). Introduction near the cathode gave substantially poorer performance.

Considerable effort has also been expended on the development of ion-chamber theory. Most of the theory has been of only moderate utility, typically describing qualitative trends with poor quantitative agreement (refs. 2, 14, 19, 43, 44, 51, 52, and 85). A thorough evaluation of published ion-chamber theory has been made recently (ref. 124). As concluded in this evaluation, the most detailed description of plasma processes and loss mechanisms has been obtained from a combination of theory and extensive probing of the ion-chamber plasma (refs. 21, 74, 97, and 113). To date, almost all progress in ion-chamber performance has been the result of cut-and-try experimentation. Ion-chamber theory, though, is reaching a level such that this empirical pattern may not be followed in the future.

The specific area of interest for the investigation reported here is propellant utilization. Propellant utilization is defined for singly ionized atoms as the fraction of total propellant flow that is ionized and accelerated into the ion beam. The earliest ion chambers reached a propellant utilization of 0.8. Shortly thereafter a scale effect was observed in which utilization was found to increase in some general manner with thruster size (ref. 14). Except for one attempt to correlate utilization data with a simple residence-time parameter (ref. 43), there were no further general advances in understanding or improving utilization. Instead, the typical approach was to improve the utilization of a specific design at a particular operating condition by largely cut-and-try methods.

The main and neutralizer cathodes have been major lifetime problems of the mercury-bombardment thruster. The main cathode has received the bulk of the attention and is considered first. The first cathode type that was used was a refractory-metal wire or ribbon. Ion bombardment was found to limit this type of cathode to lifetimes of about 1000 hours, or less, in the ion-chamber environment (ref. 29). A greater thick-

ness will be more resistant to sputtering, but cathode thickness is limited by conduction losses to supports. If the conduction losses were limited by using a heavy refractory-metal emitting surface heated by a fine enclosed filament, sublimation of the enclosed filament limits lifetime. A wide variety of matrix and dispenser cathodes (impregnated with strontium and/or barium oxides) were investigated next (refs. 31, 42, 53, 62, and 90) with the maximum lifetime exceeding 5000 hours. An oxide-coated cathode in which most of the surface is protected against energetic ion bombardment was also investigated (ref. 78). A shortcoming of any cathode that depends on oxide for most or all of its emission, though, was brought out during the SERT II program. It is desirable from a reliability viewpoint to test the actual hardware to be flown before it is launched. A tested, but unlaunched, oxide cathode is difficult to keep from exposure to the atmosphere and subsequent deactivation. This difficulty was a critical factor in the SERT II decision to use a hollow cathode (ref. 90).

The mercury hollow cathode has an interesting history. A cesium plasma-bridge neutralizer was developed for the cesium electron-bombardment thruster (ref. 143). This neutralizer was a small-scale version of the autocathode used in the ionization chamber of the cesium thruster, and its electron emission was readily explained in terms of the low work function of a cesium coating. A similar design of neutralizer was then operated on a mercury-propellant thruster (ref. 45), where the high work function of mercury made the previous explanation of operation unsuitable. During the development of the mercury plasma-bridge neutralizer for SERT II, it became evident that the neutralizer cathode would easily operate at main cathode conditions. As mentioned earlier, the switch to the hollow cathode was then made on the basis of being able to ground test the actual flight hardware. A small amount of oxide is used in the hollow cathode, but it is buried inside the cathode and is used only to provide a few microamperes of starting current. With the oxide used in this manner, repeated exposure to the atmosphere has no significant adverse effects (ref. 71). Another hollow-cathode design, now called an "enclosed keeper" design, was also considered in the early development of mercury hollow cathodes (ref. 45). This type of hollow cathode has recently shown substantial reductions over more conventional hollow cathodes in the propellant-flow requirements for low-emission applications (ref. 125).

Before leaving main cathodes, one more type should be mentioned, the liquid metal (LM) type (refs. 56, 64, and 95). The LM cathode is similar to the hollow cathode in that it can be exposed repeatedly to the atmosphere when used with mercury propellant. The LM cathode is a workable, long-lived alternative to the hollow cathode but appears to require more complex solutions to the feed and isolation problems (ref. 84). It should also be mentioned that the baffle used to control discharge voltage in the SERT II thruster with a hollow cathode had its origin in a similar baffle used in ion chambers with LM cathodes.

The first neutralizers used with bombardment thrusters were simple refractory-metal thermionic emitters that were immersed in the ion beams (refs. 1 and 23). Such neutralizers are satisfactory for short tests, such as the SERT I ballistic flight (ref. 39), but ion erosion prevents their use for long-duration applications. Thermionic cathodes have also been placed near the ion beam, but such placement has always been a compromise between ion impingement from the fringe of the ion beam and high losses due to poor coupling to the beam (ref. 55). The plasma-bridge neutralizer avoids, this compromise by providing ions to neutralize the electron space charge (refs. 83, 86, 89, and 131). Thus, the plasma-bridge neutralizer can be located well out of the ion beam and still operate with small coupling losses.

The accelerator system that is presently used on most electron-bombardment thrusters consists of parallel plates with matching hexagonal arrays of holes and held in relative position by shadow-shielded ceramic insulators around the outside of the structure. Extensive experimental tests have been conducted on this type of accelerator system (refs. 13, 25, 41, and 61). Unlike ion-chamber theory, acceleratory theory has been well understood for a long time. The major cause of wear in a well-designed accelerator is charge-exchange erosion (ref. 22). The calculation of ion trajectories is well understood - although complicated and tedious. Because of the difficulty of making ion-trajectory calculations, early accelerator designs were created by empirical methods. The availability of electronic computers and ion-trajectory programs, though, has made the theoretical approach much easier to use (ref. 105).

Another type of accelerator system uses only one metal grid with a nonconducting coating on the side of the grid facing the ion chamber (refs. 54, 75, and 102). This composite accelerator is particularly sensitive to backsputtered metal from the ion-beam target and has not yet reached the reliability and durability of more conventional accelerators. The composite accelerator originated from discussions at the Lewis Research Center of an early version of a radiofrequency ion thruster developed by Löb (ref. 157). The thruster discussed had a conventional metallic accelerator, but there was an insulator in contact with the accelerator to take the place of the usual screen grid. This sharp departure from conventional electron-bombardment accelerator construction stimulated a series of experiments that ended in the construction of the first one-piece composite accelerators (ref. 54).

There is a significant interaction between the ion source and the accelerator system. One aspect is the effect of screen-grid - open-area fraction, with the largest open-area fraction giving the lowest ion-chamber loss (ref. 60). Another aspect is the relation between ion-beam current and the current capacity of the accelerator system. For a given beam current and total propellant flow rate, the ion-chamber losses are lowest for an accelerator system operated at a small fraction of its current capacity. This last aspect has been shown by varying the voltage of a single accelerator configuration (ref. 12) and by a more general correlation of similar configurations (ref. 87).

Other components and aspects of electron-bombardment thrusters that have been investigated are feed systems (refs. 15 and 46) isolators (refs. 34, 49, and 77), arcing (refs. 20 and 33), and controls (refs. 28, 35, 66, and 127). The effluents of the thruster have also been studied, first from the diagnostic viewpoint (refs. 38 and 45) and later from the viewpoint of interactions with the rest of the spacecraft (refs. 72, 104, 107, 122, 133, 135, and 140). Although the bulk of published electron-bombardment development has taken place in the United States, considerable work has also been done in Europe (refs. 63, 68, 81, 93, 98, 129, and 141).

Present Investigation

The objective of the present investigation is to determine the factors that control maximum utilization of propellant in an electron-bombardment thruster. The thrust in a space propulsion application is provided almost entirely from the ionized portion of the propellant. The un-ionized propellant thus constitutes a loss and should be minimized. The only previously published attempt to predict propellant utilization (ref. 43) used a residence-time approach for a neutral in the ion chamber. Although this approach gave the correct qualitative trends, quantitative agreement was poor. The objective of this investigation, then, includes obtaining a quantitative agreement better than that previously published. An analysis of maximum propellant utilization was published earlier as part of the investigation described in this report (ref. 136) and is the foundation for the theory which will be compared with experimental data.

The thruster selected for the experimental portion of the investigation was originally operated with a 20-centimeter-diameter accelerator system but was masked down to a 10-centimeter system for the work described in this report. This thruster permitted tests over a wide range of ion-chamber configurations, including ones with diameters larger than the accelerator system. An electromagnet was used instead of permanent magnets to permit a range of field strengths to be investigated. A strongly divergent magnetic field (with field-shaping pole pieces) was employed to be consistent with current design trends. Each ion-chamber configuration was operated over a wide range of propellant flow rates from near the lower limit for a sustained discharge to near the upper limit controlled by frequent electrical breakdowns. The thruster was operated in vacuum chambers located at Colorado State University and at the NASA Lewis Research Center. SI (mks) units are used throughout this report.

ION-CHAMBER THEORY

The operation and typical values of various operating parameters are presented in the first part of this section. The two propellant-utilization theories that are compared to the experimental data are also presented, as well as a discussion of the Bohm criterion and its use in this investigation.

Typical Operation

A schematic of an electron-bombardment thruster is shown in figure 1. Electrons are emitted by the ion-chamber cathode, which is maintained 30 to 40 volts negative of the anode. The emitted electrons are constrained by the magnetic field (not shown in fig. 1) until they collide with propellant atoms. The magnitude of the cyclotron radius for high-velocity emitted electrons is typically 0.1 to 0.5 of the ion-chamber radius.

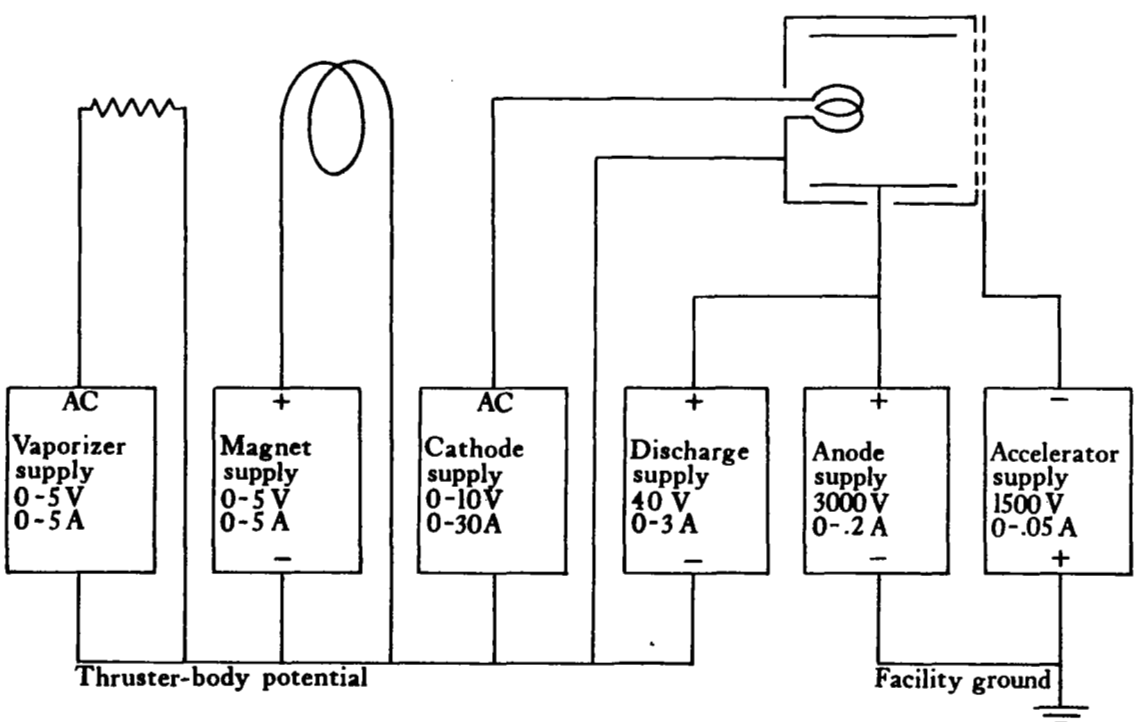

Figure 1. - Schematic diagram of electron-bombardment thruster with power supplies.

Some of the ions produced by these collisions reach the right end of the ion chamber, where they are accelerated to form the ion beam. This ion beam is normally charge-density and current neutralized in space by electrons emitted by the neutralizer cathode. In this investigation no neutralizer was used. Instead, as is frequently done in ground tests, the secondary electrons from the ion-beam target were used to charge neutralize the ion beam. The low density and high velocity of the ions in the ion beams assure that only a negligible fraction of the ions recombines with electrons near the thruster.

Un-ionized propellant atoms also escape through the accelerator and are the loss of particular interest in this investigation. Thruster efficiency is defined as

$$\eta_T = \frac{F^2}{2\dot{m}P} \tag{1}$$

where F is the thrust in newtons, $\dot{m}$ is the total propellant flow in kilograms per second, and P is the power in watts. In terms of the propellant flow $\dot{m}_i$ that is ionized and ejected from the thruster and the propellant utilization $\eta_U (= \dot{m}_i/\dot{m})$, equation (1) can be rewritten as

$$\eta_T = \frac{\eta_U F^2}{2\dot{m}_i P} \tag{2}$$

The thruster efficiency is thus proportional to propellant utilization, and an improvement in propellant utilization can be translated directly into improved thruster performance. The understanding that might make possible such a performance improvement is the objective of this investigation.

During typical operation the neutral density in the ion chamber corresponds to about 10^{-4} torr, or $\sim 10^{18}$ mercury atoms per cubic meter at a 500 K ion-chamber wall temperature. The ions are only about 10 percent as dense as the neutrals ($\sim 10^{17}/m^3$), and the electron density equals that of the ions (ref. 123). All of these densities are approximate mean values for the ion chamber as a whole when operated at design conditions. Special locations such as the vicinity of a hollow cathode could exhibit large departures from the values given. The electron energy distribution corresponds to roughly a 5-eV temperature, although there are significant departures from a Maxwellian distribution that are discussed later in this report. This approximately 5-eV temperature is the result of energy addition (directly or indirectly) by emitted electrons and energy loss by excitation and ionization.

The Debye shielding distance for a plasma in which most of the random energy is in the electron population ($T_e \gg T_i$) is

$$l_D = 7.43\times10^3 \sqrt{\frac{T_e}{n_e}} \tag{3}$$

where T_e is the electron temperature in eV, and n_e is the electron density in number per cubic meter. For typical ion-chamber conditions, equation (3) gives $\sim5\times10^{-3}$ centimeter. This small Debye shielding distance, when compared with the ion-chamber diameter of 10 centimeters, justifies the assumption of $n_e = n_i$.

Although the ion density is normally much less than the neutral density in the ion chamber (ref. 97), far more ions than neutrals leave through the accelerator system. This apparent discrepancy is due to the difference in velocities for these two species in the ion chamber. The neutral velocity distribution is essentially Maxwellian and is controlled by the wall temperature. The average magnitude of neutral velocity ($\bar{v}_o = \sqrt{8kT/\pi m}$) is 230 meters per second for a typical wall temperature of 500 K. The loss rate of neutrals $\dot{N}_o$ can be calculated from

$$N_o = \frac{n_o \bar{v}_o A_o}{4} \tag{4}$$

where n_o is the neutral density in the ion chamber, and A_o is the equivalent sharp-edged orifice area of the accelerator system. The ions, on the other hand, have a directed velocity towards the boundaries of the ion chamber, including the accelerator system. This directed velocity is given by Bohm's criterion for a stable sheath (ref. 158),

$$v_i \geq \sqrt{\frac{q_i T_e}{m_i}} \tag{5}$$

where q_i and m_i are the charge and mass of the ions. Expression (5) is equivalent to the ions having a minimum energy equal to one-half that of an electron at the most probable velocity ($v_{mp} = \sqrt{2kT/m}$). Expression (5) indicates a range of ion velocity is possible. In practice, though, an equality is generally assumed. This use of an equality is discussed later in this section. There are corrections that can be given to the minimum velocity of expression (5). One correction that has been made is due to the departure of electrons from a Maxwellian distribution (ref. 123). Another more difficult correction, that apparently has been done only in a simplified form (ref. 159), includes the effect of ions coming from different regions at different potentials, and thus having a range of ion velocities. To apply the first of these corrections to the investigation of this report requires a completeness of probe data that has seldom been attained. To

apply the second would require laborious detailed calculations based on such complete probe data. Because of the directed nature of this Bohm velocity, the relation for loss rate of ions is essentially

$$\dot{N}_i = n_i v_i A_i \tag{6}$$

where n_i is the ion density, and A_i is the boundary area involved in ion loss. (The area A_i is usually several times larger than the neutral-loss area A_o used in eq. (4).) For an electron temperature of 5 eV, the Bohm velocity for singly charged mercury ions is 1.55×10^3 meters per second. With this velocity, equation (6) indicates a loss rate of ions about a factor of 10 greater than that for neutrals (eq. (4)). The low fraction of ionization in the ion chamber is thus quite compatible with a high fraction of ions in the particles escaping through the accelerator system.

The ion-chamber plasma is assumed in the foregoing to have all path lengths long compared to ion-chamber dimensions. The mean-free-path length for electrons colliding with neutrals or for energetic electrons colliding with slower background electrons is given by

$$l = \frac{1}{n\sigma} \tag{7}$$

where n is the density of the target species, and σ is the cross section of the process. The path length for the total collision cross section of electrons with neutrals is about 1 to 3 meters for an electron energy range of 5 to 40 eV. The large magnitude of this path length compared with ion-chamber size is the reason for using a magnetic field to conserve electrons. The magnetic field is weak enough ($\sim 10^{-3}$ T, or ~ 10 G), though, that the ion trajectories are essentially unaffected.

The cross section for excitation or ionization by 30- to 40-eV electrons is about 5×10^{-20} square meter (refs. 160 and 161), which gives a path length of about 20 meters. The electron-electron coulomb-collision cross section (90° collision) for 30- to 40-eV electrons and a $\sim 10^{17}$-per-cubic-meter background electron density is also about 5×10^{-20} square meter (ref. 162), but the electron density is lower than the neutral density so that the path length for this process is about 200 meters. Thus, the probability of energy loss due to excitation and ionization for a 30- to 40-eV electron is much greater than that due to coulomb collisions with back-ground electrons. The population of these energetic electrons, then, is determined by cathode emission rather than a Maxwellian "tail." As a rough approximation perhaps 10 percent of the electrons are usually found to be energetic "primaries," while the rest make up an essentially Max-

wellian distribution.[1] The primary electrons have been found to produce about half the ions in the ion chamber, while the Maxwellian "tail" produces the rest (ref. 123). This division of ion production is for normal operation and will be a subject of discussion for conditions of maximum utilization.

Metastable states are often important in mercury discharges. Because of the low pressure of the discharge, though, metastable states are not important for ion production in a bombardment ion thruster.

Residence-Time Approach

The residence-time approach described in this section was published in 1965 (ref. 43). It assumes a cylindrical ion chamber with an accelerator system covering one end of the cylinder and with uniform conditions throughout the chamber. The differential equation for probability of ionization p_i is

$$dp_i = v_e \sigma t_o (1 - p_i) dn_e \tag{8}$$

where σ is the ionization cross section, t_o is the residence time for a neutral (in the absence of ionization) in the volume of interest for production of beam ions, and n_e and v_e are the density and velocity of the ionizing electrons. The probability p_i can be integrated from 0 to η_U, while the electron density is integrated from 0 to n_e. This gives propellant utilization η_U as

$$\eta_U = 1 - \exp(-n_e v_e \sigma t_o) \tag{9}$$

Thus $n_e v_e \sigma t_o$ can be used as a correlating parameter for propellant utilization. The variables used in this parameter, though, are not particularly convenient. More accessible variables will therefore be substituted. The mean electron energy can be assumed proportional to the ionization potential φ_i, inasmuch as the electron energy is normally controlled by excitation of ground-state neutrals, and the excitation energy of ground-state neutrals is roughly proportional to φ_i. Thus, the electron velocity is

$$v_e \propto \varphi_i^{1/2} \tag{10}$$

[1]This is one of the important differences between cesium and mercury electron-bombardment thrusters. The electron-electron coulomb-collision cross section varies inversely as the square of electron energy. The much lower discharge voltages used with cesium thus result in very rapid randomization of emitted electrons, with no distinct primary electron group.

The electron density can be expressed in terms of the ion density upstream of the accelerator, which in turn can be expressed in terms of the ion-beam current density j_i and the Bohm critical velocity. With these assumptions, one finds

$$n_e \propto \frac{j_i w^{1/2}}{\varphi_i^{1/2}} \tag{11}$$

where w is the atomic weight of the propellant. The residence time is a function of neutral velocity ($v_o \propto w^{-1/2}$) and ion-chamber length l, so that

$$t_o \propto l w^{1/2} \tag{12}$$

From the last three relations, the correlating parameters can be written as

$$n_e v_e \sigma t_o \propto j_i l \sigma w \propto j_i l \tag{13}$$

(The last step results from the propellant being restricted to mercury in this investigation.) Equation (9) can therefore be written as

$$\eta_U = 1 - \exp(-K j_i l) \tag{14}$$

where K is a constant that can be evaluated from the previously published analysis (ref. 43) as 5.2.

For equation (14) to correlate the performance of different thrusters, various conditions (such as ion-chamber wall temperature and fraction blockage of the accelerator system) must be nearly the same for different thrusters. In particular, the use of a 20-centimeter chamber diameter with a 10-centimeter accelerator system is a sharp departure from the conditions assumed for this equation. In fact, only the 10-centimeter chamber data presented in this report are suitable for comparison with equation (14). Inasmuch as these last mentioned data will still be found to correlate poorly with equation (14), there will be no need to modify that equation for the 20-centimeter-chamber data.

Primary-Electron-Region Approach

This analysis is directed at a condition of high propellant utilization and is concerned for the most part with primary electrons. The primary electrons do not occupy

the entire ion chamber, but instead are concentrated in only a portion of the volume. This portion is essentially restricted to the volume enclosed by the accelerator system and magnetic-field lines that intersect the anode. The reason for this restriction of primary electrons to a small volume is that the small plasma sheath on the anode does not reflect energetic electrons that can reach it. The existence of a primary-electron region is experimentally evident when detailed probe data are available (ref. 123). At the high-utilization condition of interest in this analysis, a high fraction of primary electrons is expected. The high fraction of primary electrons is in turn expected to result in primaries causing the bulk of ionizations. The expectation of a high fraction of primaries is supported by probe data.

Early bombardment-thruster designs typically had an extensive volume occupied by primary electrons, as indicated in figure 2. Because the region occupied by primary electrons in this design extends the full length of the ion chamber, a change in ion-chamber length will clearly affect the primary electrons. The primary-electron region indicated in figure 2 is, of course, somewhat idealized. The finite cyclotron radius of primary electrons leads to a boundary with finite thickness instead of the line thickness of a limiting magnetic-field line, as indicated in figure 2. With recent divergent-field designs, however, the primary-electron region is localized near the screen. For the thruster under investigation in this report, the primary-electron region is indicated in figure 3. As shown in figure 3, the primary-electron region is independent of chamber geometry unless the chamber is made very short.

The density of primary electrons increases with discharge current. For a rough approximation, then, the limiting condition of all electrons being primaries can be assumed for maximum utilization. Consider first the total ion production rate $\dot{N}$ from primary electrons. When mean values are used for the primary-electron region,

$$\dot{N} = n_p v_p n_o \sigma V_p \tag{15}$$

where n_p and v_p are the primary-electron density and velocity, n_o and σ are the neutral density and ionization cross section, and V_p is the volume of the primary-electron region. For the total loss rate of ions from this region,

$$\dot{N} = n_i v_i A_p \tag{16}$$

where n_i and v_i are the ion density and velocity toward the outer boundary of the primary-electron region, and A_p is the area of this outer boundary. The ion velocity toward the outer boundary can be estimated from the Bohm criterion for a stable sheath given in expression (5), in which a Maxwellian electron distribution is assumed. The limiting condition of all electrons being primaries would probably depart from a Maxwellian distribution, but expression (5) should still approximate the sheath stability limit.

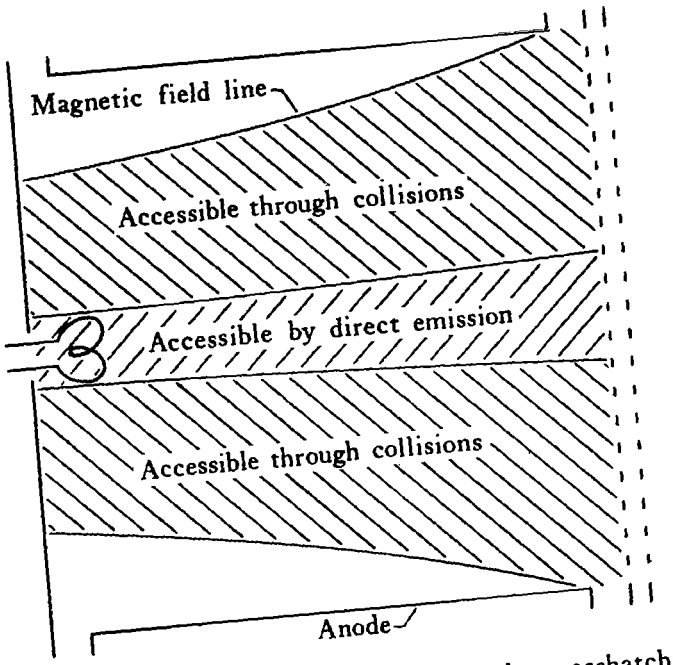

Figure 2. - Primary-electron region (shown by crosshatching) of early bombardment thruster. CS-58229

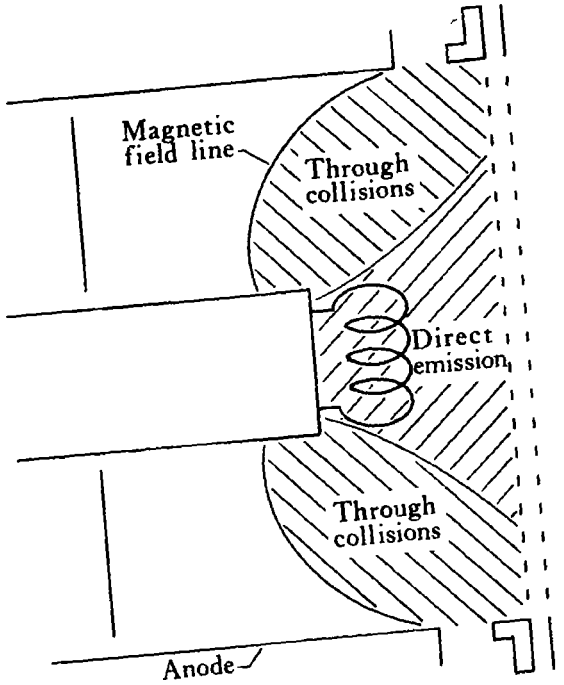

Figure 3. - Primary-electron region (shown by crosshatching) of divergent-field thruster used in this investigation.

For the limiting condition of all electrons being primaries and the mean energy used for T_e, the minimum ion velocity from expression (5) is

$$v_i = v_p \sqrt{\frac{m_e}{2m_i}} \tag{17}$$

As mentioned earlier, the Debye shielding distance is very small. For the primary-electron region, then, with all electrons in this region assumed to be primaries,

$$n_p = n_i \tag{18}$$

With the substitution of equations (17) and (18) into (16) and the equating of ion loss and production rates (eqs. (15) and (16)), one finds

$$n_o = \frac{\sqrt{m_e/2m_i}}{\sigma(V_p/A_p)} \tag{19}$$

With mercury used for m_i and 5×10^{-20} square meter used for the ionization cross section σ (40-eV electrons), this becomes

$$n_o = \frac{2.34\times10^{16}}{V_p/A_p} \tag{20}$$

A constant neutral density upstream of the accelerator system implies a constant loss of neutrals at maximum propellant utilization regardless of the total mass flow.

The preceding part of this approach (eqs. (15) to (20)) has been published previously (ref. 136). The following extension has been made in an attempt to approximate more closely the effects of a non-Maxwellian electron distribution. This extension includes the effects of both primary and Maxwellian electrons.

A modified Bohm criterion has been derived by Masek to give the combined effect of monoenergetic primary and Maxwellian electron populations (refs. 97 and 123). This modified Bohm criterion can be written (at the minimum ion energy) as

$$v_i = v_m \sqrt{\frac{m_e(n_p + n_m)}{2m_i n_m}} \tag{21}$$

where v_m is the most probable Maxwellian electron velocity ($v_{mp} = \sqrt{2kT/m}$), and n_p and n_m are the primary and Maxwellian electron densities. Equation (21) can be rewritten as

$$v_i = v_p \sqrt{\frac{m_e}{2m_i}} \sqrt{\frac{T_m}{\mathscr{E}_p}} \sqrt{1 + \frac{n_p}{n_m}} \tag{22}$$

where v_p is the primary-electron velocity, and T_m and $\mathscr{E}_p$ are the Maxwellian electron temperature and primary-electron energies, both in eV. Equation (18) can be rewritten in terms of primary and Maxwellian electron populations as

$$n_i = n_p \frac{1 + n_p/n_m}{n_p/n_m} \tag{23}$$

Substitution of equations (22) and (23) into the loss-rate equation (eq. (16)) yields

$$N = n_p v_p \sqrt{\frac{m_e}{2m_i}} \sqrt{\frac{T_m}{\mathscr{E}_p}} \frac{(1 + n_p/n_m)^{3/2}}{n_p/n_m} A_p \tag{24}$$

Equation (15) can be used again for the production-rate equation. Equating the loss and production rates,

$$n_o = \frac{\sqrt{m_e/2m_i}}{\sigma(V_p/A_p)} \sqrt{\frac{T_m}{\mathscr{E}_p}} \frac{(1 + n_p/n_m)^{3/2}}{n_p/n_m} \tag{25}$$

The mass of a mercury ion can be assumed for m_i, and 5×10^{-20} square meter can be used for σ. A value of 5 eV is reasonable for T_m, while ~40 eV would be expected for $\mathscr{E}_p$ in a 40-volt discharge (used throughout this investigation). Equation (25) can then be written as

$$n_o = \frac{0.827 \times 10^{16}}{V_p/A_p} \frac{(1 + n_p/n_m)^{3/2}}{n_p/n_m} \tag{26}$$

The variation of $n_o(V_p/A_p)$ as a function of n_p/n_m was obtained from equation (26) and plotted in figure 4. The value of $n_o(V_p/A_p)$ from equation (26) is seen to be higher than

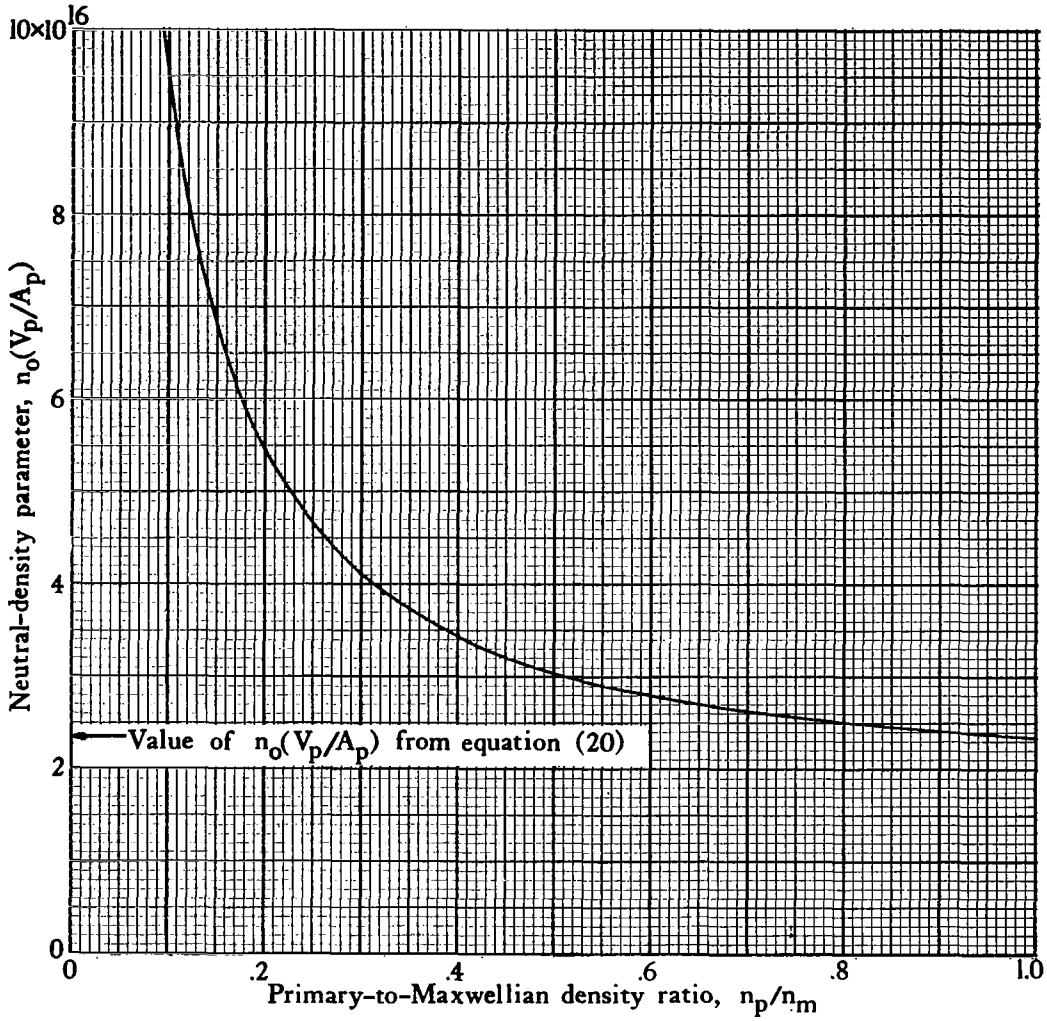

Figure 4. – Variation of neutral-density parameter with primary-to-Maxwellian density ratio – from equation (26). Primary energy, 40 eV; Maxwellian temperature, 5 eV.

the same value from equation (20) for all $n_p/n_m < 1$. Because of its inclusion of non-Maxwellian electron-distribution effects, equation (26) is thought to be more accurate than equation (20).

Use of Bohm Criterion

The Bohm criterion plays an important role in the preceding analysis. Some additional comments on the use of this criterion therefore appear to be appropriate. The original relation given for this criterion of sheath stability was (ref. 158)

$$v_i \geq \sqrt{\frac{q_i T_e}{m_i}} \tag{27}$$

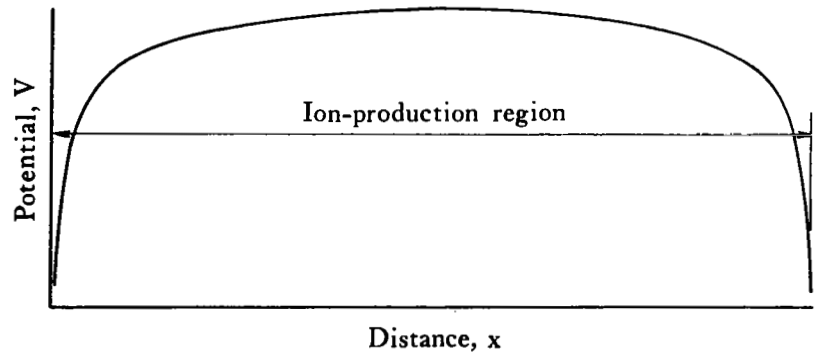

(a) Ion production throughout.

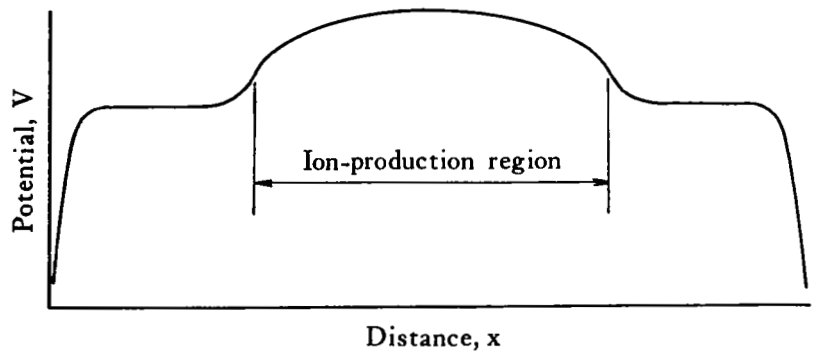

(b) Localized ion production.

Figure 5. - Form of potential solutions for low-density plasma.

That is, the directed velocity of (cold) ions toward a collisionless sheath must be equal to, or greater than, the critical value of $\sqrt{q_i T_e/m_i}$. In making ion-flux calculations for a sheath, however, it is customary to assume a simple equality. Perhaps the best justification for such an assumption is that it gives results in agreement with experiment (refs. 97 and 123). Another assumption in the preceding analysis is the use of the Bohm criterion at the upstream boundary of the primary-electron region. This boundary is not a sheath in the ordinary sense. It is, instead, a boundary that separates the primary-electron region with its high ion production rate from the rest of the ion chamber with a much lower ion production rate. This assumed difference in ion production rate is supported in the RESULTS AND DISCUSSION section by Langmuir probe data.

To see the effect of localizing the ion production region, consider figure 5. In figure 5(a) the ion production extends throughout the region between two walls and shows the customary gradual transition from plasma to sheath. In figure 5(b) the ion production has been localized to a central portion of this region. The solution shown in figure 5(b) has been obtained analytically (ref. 163). The ions were found in this analysis to have close to the critical velocity of $\sqrt{q_i T_e/m_i}$ throughout the two regions of nearly uniform potential shown in figure 5(b). From figure 5(b), then, one would expect the Bohm criterion to apply to the boundary of the primary-electron region as long as the bulk of ion production takes place in this region.

APPARATUS

The mercury propellant thruster used in this investigation is shown in figure 6. The magnetic field is determined by a ring-shaped soft-iron pole piece near the accelerator and a cylindrical soft-iron pole piece near the cathode. These pole pieces are connected by four soft-iron paths (each about 3.2 by 12.7 mm, in cross section) on which the field windings are mounted. The cylindrical pole piece has about the same cross section as the total of the four paths and also has a field winding for most of its length. There were about 5.3 turns per centimeter for all of the field windings. The construction of the four soft-iron paths permitted axial motion of the cylindrical pole piece for initial optimization. Thereafter, the cylindrical pole piece was held fixed. The data presented in this report were obtained with the central pole piece 3.5 centimeter from the screen grid. This axial location gave good performance over a wide range of utilization. Experimental data were taken at various magnetic-field currents, but most of the data were obtained at a current of 1 ampere. At this current the typical magnetic field in the ion chamber (assumed to be midway between probes A and B in fig. 7) was about 3×10^{-3} tesla (30 G). This field was somewhat nonlinear with current and rose to about 5×10^{-3} and 9×10^{-3} tesla for currents of 2 and 5 amperes.

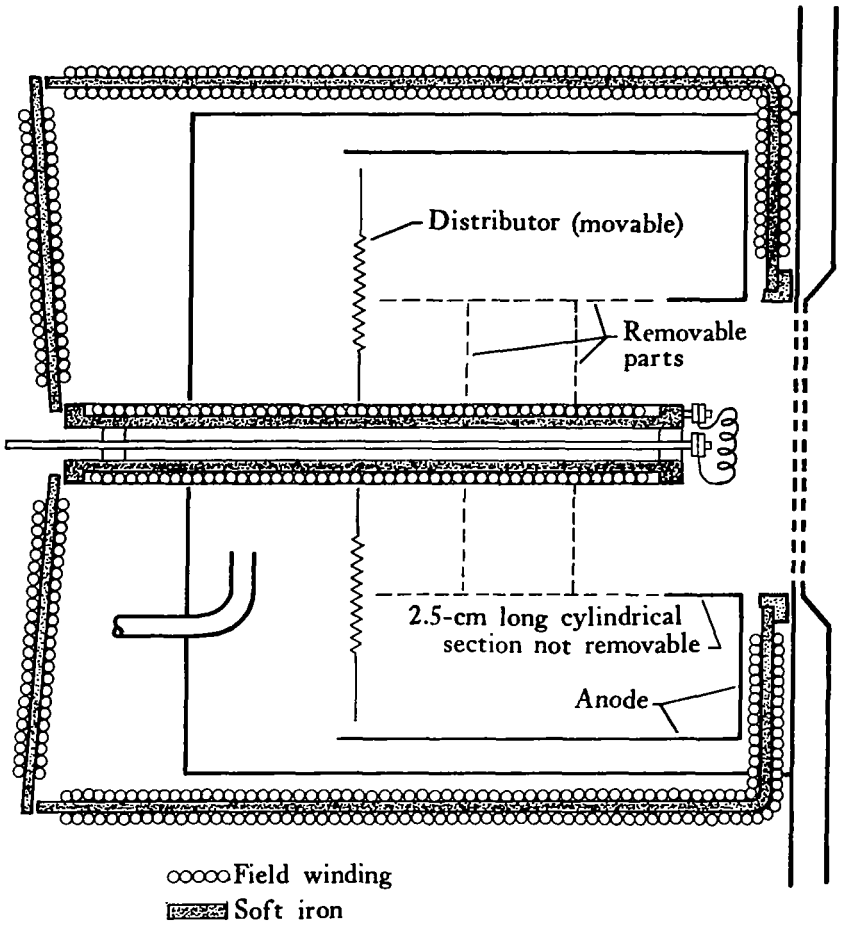

Figure 6. - Thruster with adjustable ion chamber. CS-58226

A screen with 71 percent open area was used to reduce ion recombination on the screen. Only holes completely within a 10-centimeter-diameter circle were used to accelerate ions, and there were 429 such holes in the accelerator design used. The screen-accelerator spacing was 2 to 2.5 millimeters over the beam area. A tungsten wire cathode was used to avoid both (1) the uncertainty in propellant utilization that can occur when an oxide cathode is inadvertently overheated, and (2) the effect of localized propellant concentration associated with a hollow cathode.

Ion-chamber probes were made by using 0.75-millimeter tantalum wire inside aluminum oxide tubes with an outside diameter of 1.6 millimeters. The locations of the probes are shown in figure 7. The two probes closest to the accelerator (A and B in fig. 7) were constructed with 0.75 millimeter of tantalum wire extending beyond the aluminum oxide. Probe C, because of the lower plasma density in that location, was constructed with a 1.5-millimeter extension. Probe location selections were made

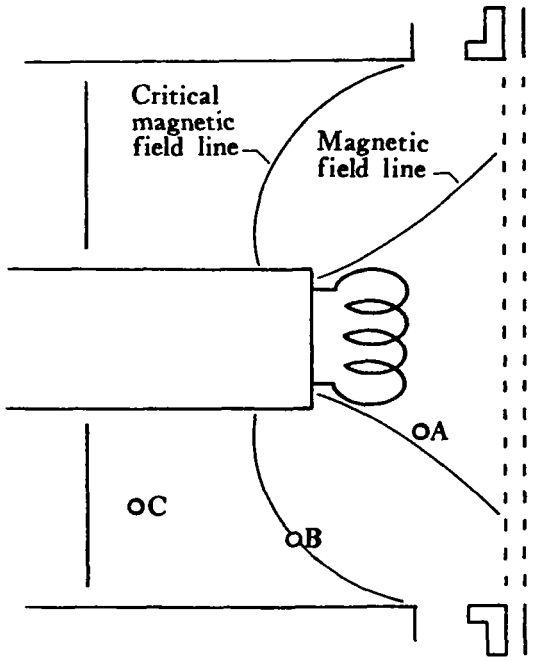

Figure 7. - Probe locations in ion chamber.

based on published probe surveys (refs. 85 and 97). Probe A intersected a magnetic-field line near the edge of the cathode and was thought to be representative of the primary-electron region. Probe B intersected a magnetic-field line at the boundary of the primary-electron region, while probe C was well removed from that region. Quartz tubes were used for one set of probe data in an attempt to extend the range of the probe data to higher propellant mass flows by reducing outgassing. Tantalum wires of 0.5-millimeter diameter (in holes of approximately the same diameter) were mounted flush with the ends of the quartz tubes in this set.

The thruster was first operated in a 1.2-meter-diameter, 4.8-meter-long Space Propulsion Research Facility located at Colorado State University. Most of the data, including all the probe data, were obtained during later operation in a 1.5-meter-diameter, 4.2-meter-long vacuum chamber at the NASA Lewis Research Center. Sketches of these two facilities are shown in figure 8. Both facilities used liquid-nitrogen-cooled liners and oil-diffusion pumps to attain pressures in the 10^{-6} torr range. In both cases the thruster was mounted in the bell jar shown at the left end of the facility. Existing power supplies were used for the various thruster functions at both facilities,

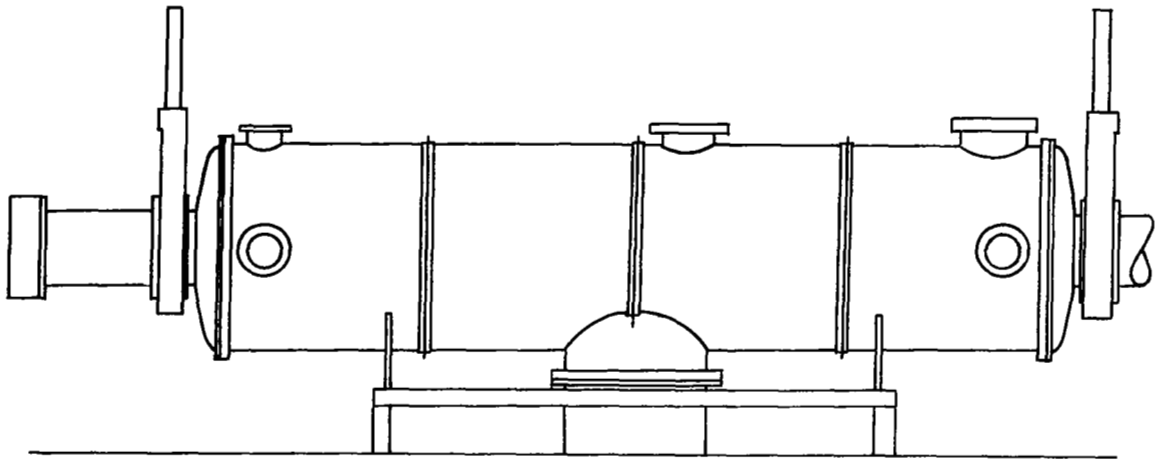

(a) Facility at Colorado State University.

CS-58223

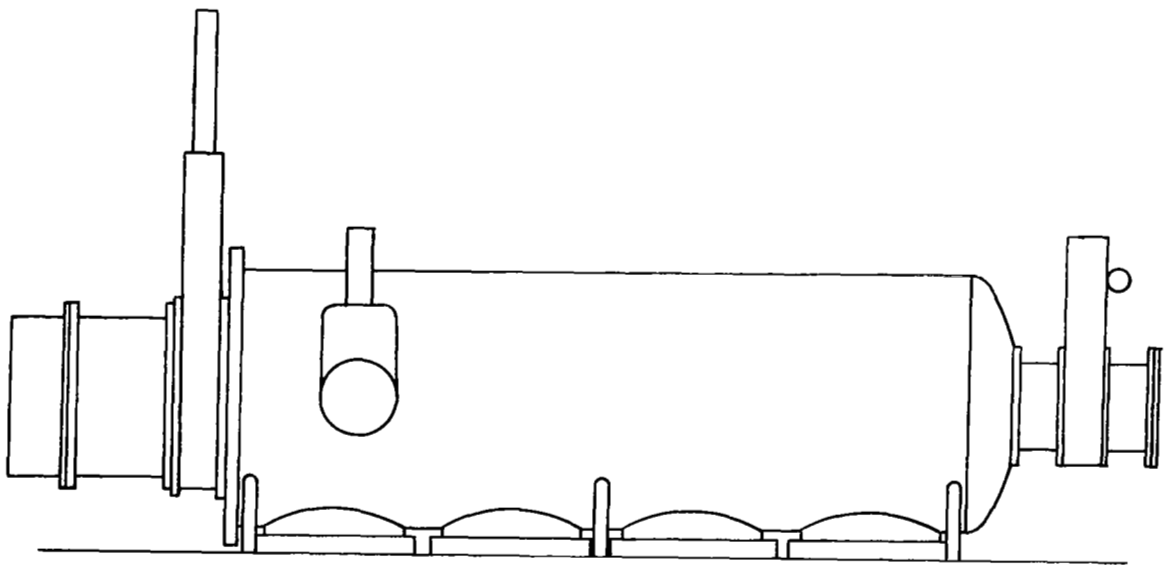

(b) Facility at Lewis Research Center.

Figure 8. - Vacuum facilities used in this investigation.

and the propellant flow at both locations was measured by timing the drop of a mercury column in a calibrated glass tube.

The meters used in voltage and current measurements are accurate within ±2 percent of full scale. Typical part-scale measurements should therefore be within ±5 percent. Because of the electrical transients that occur in other circuits when the accelerator system arcs, frequent calibration is necessary. The glass propellant-flow tube has a bore variation of 2 to 3 percent. This variation, together with a maximum of about 1 percent uncertainty in column-height measurement, determines the accuracy of the mercury-flow measurement.

PROCEDURE

The thruster used was unusual in that a thruster body suitable for a 20-centimeter-diameter accelerator system was used with only a 10-centimeter system. Because of this thruster design, the ratio of thruster mass to discharge power was large. This large mass resulted in the slow starting transient shown in figure 9. The 0.5-ampere discharge was started at time zero in figure 9. The high voltages were applied 2 minutes after the discharge was started, but did not reach the values of 3000 and -1500 volts until 12 minutes after the discharge was started. Condensation of propellant was assumed to have taken place on internal thruster surfaces before the thruster discharge was started. Evaporation after the ion-chamber discharge was started would then account for the rapid rise and large peak in ion-beam current. Equilibrium operation was attained when the condensed propellant was all evaporated, which apparently took about $1\frac{1}{2}$ hours. The bumps in the descending curve of figure 9 were typical and apparently resulted from different parts of the thruster becoming warm enough to vaporize the condensed propellant at different times.

There was also a short-term transient effect whenever discharge conditions were changed. This effect was found after the initial warmup and was presumably due to the large ratio of internal surface area to beam area. Because of the adsorption of propellant on these surfaces at pressures of the order of 10^{-4} torr, a few minutes were required to reach equilibrium when the ion-beam current was changed. The associated transient effect is shown in figure 10, where a hysteresis loop is shown that was obtained by rapidly changing the discharge current (one data point per min). Some data in the first paper of this investigation (ref. 136) were taken without sufficient operation at each condition to avoid this effect. For the data presented here the thruster was operated for at least 5 minutes at any conditions that involved a substantial change in beam current from the previous operation point.

A transient thermal effect was also evident in the propellant flow measurement. A mass flow was set by holding the vaporizer constant ($\pm 1^{\circ}$ C) at some temperature. The

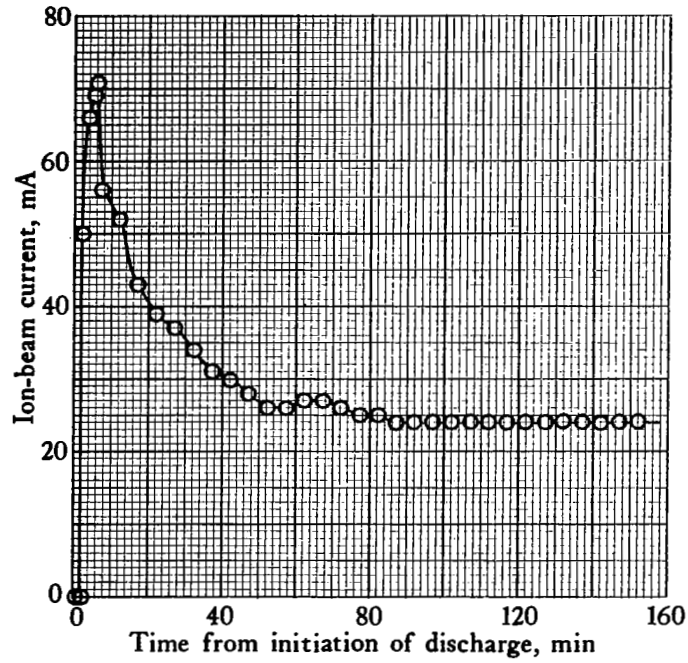

Figure 9. - Starting transient for discharge (anode) current of 0.5 A and total propellant flow of 78 mA equiv.

CS-58220

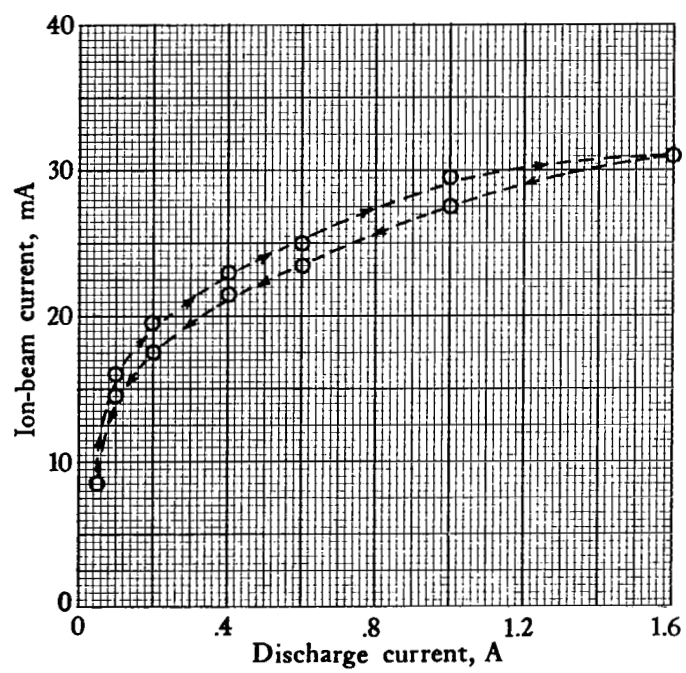

Figure 10. - Short-term transient (1 min between data points) for total propellant flow of 74 mA equiv.

CS-58222

flow was then determined by measuring the drop in height of a mercury column and the time required for this drop. To assure an accurate measurement of this column drop despite meniscus effects in an approximately 1-millimeter bore, a drop of about 4 centimeter or more was used at any vaporizer temperature. To obtain reproducible readings after any change in vaporizer temperature, though, a wait of about 15 minutes was found necessary.

All steady-state operation was at an anode potential of 3000 volts and an accelerator grid potential of -1500 volts, with both measured relative to the vacuum facility. The acceleration potential difference of 4500 volts was sufficient to handle ion-beam currents of at least 150 milliamperes without any substantial rise in impingement.[2] No neutralizer was used, and charge-density neutralization of the ion beam was obtained by secondary electrons from ions striking the various portions of the facility.

The discharge chamber was operated at a potential difference of 40 volts for all data presented herein. A range of cathode emissions was obtained for each of several mass flow rates. The cathode emission was limited on the high end of the range by extinguishing the discharge, reaching the space-charge emission limit of the cathode, or simply approaching the heater power limit of the cathode. The space-charge limit on emission is reached when an increase in heater power results in little or no increase in emission. A check point of one of the initial points was usually taken after covering a range of emission currents. This procedure provided a spot check on constancy of other variables while emission-range data were obtained.

Propellant flows were limited on the low end by inability to sustain a discharge at 40 volts and at the high end by repeated electrical breakdowns between the screen and accelerator grids. This range of propellant flow (and emission) was investigated with each of the ion-chamber configurations.

The ion-chamber configurations were limited to three different lengths (7.2, 10.8, and 14.4 cm) with a 10-centimeter diameter and two different lengths (9.4 and 14.4 cm) with the larger 20-centimeter diameter. These configurations provided a range of about 4:1 for ion-chamber wall area and about 8:1 for volume. The propellant introduction to the ion chamber was controlled by baffles of polyimide sheet. Most of the data were obtained in the usual mode of straight-through flow from one end of the ion chamber to the accelerator on the other end. This mode is called "forward feed." For comparison,

[2]The current to the accelerator is usually called "impingement" in mercury thruster work, because a low secondary-electron emission (10 percent or less) is the only difference between the charge carried by ions striking the accelerator and the measured current. In cesium thruster work it is customary to refer to this current as a "drain." This is because a cesium coating on a hot accelerator electrode can result in electron emission currents much greater than the ion impingement current.

one configuration was operated with "reverse feed," where the propellant was introduced through the gap between the ring-shaped pole piece and the anode.

Most of the data were obtained at a magnetic-field current of 1 ampere, which provided a compromise between good performance at high mass flow and ability to operate at low mass flow. Some data were also obtained at higher fields, though, for comparison.

Ion-chamber probe runs were made after runs of the same configuration without probes. This procedure permitted the time-consuming probe data to be obtained at a few preselected operating conditions, instead of determining the range of operation at the same time as obtaining the probe data. It also permitted a check on overheating of the probe insulation through the effect of the resultant outgassing on beam current and comparison with ion-chamber performance obtained without probes. Early runs showed that the probes became coated with a conducting layer after 2 to 3 days of operation, which led to erroneous probe data. To avoid this probem, probe insulators were discarded after 1 day of operation (in addition to being checked with an ohmmeter after each run to verify that there was no conducting layer). The use of aluminum oxide tubes led to a propellant-flow limitation where (at high discharge power) outgassing occurred because of overheating. In an attempt to extend the probe data to higher flows, the aluminum oxide tubes were replaced with quartz tubes. Although this substitution avoided the outgassing problem, the higher cathode sputtering at higher flows led to more rapid coating of the probe insulators with conducting layers. Thus, no significant extension of the probe data was obtained by this substitution. This probe limitation is apparently avoided with oxide-coated and hollow cathodes, inasmuch as probe data have been obtained at higher neutral flows with these cathodes (refs. 21, 74, 97, and 113).

In addition to the data checks described, the effects of multiple ionization and neutral backflow from the vacuum facility were also considered, though not included. A study of multiple ionization has shown that the ion-chamber discharge voltage and the cross sections for single and double ionization can be used to predict the fraction of doubly ionized atoms (ref. 16). The cross section for single ionization by a 40-eV electron is about 5×10^{-20} square meter, while the cross section for double ionization by an electron of that energy is about 1×10^{-21} square meter (refs. 160 and 161). The fraction of doubly ionized atoms should therefore be about 0.02. The appearance potential for triply ionized mercury is over 63 eV; hence, no triply ionized atoms would be expected. The reasons for this experimental result are that most beam ions come from collisions of primary electrons, and that these ions leave the ion chamber so rapidly after being ionized that there is little probability of additional ionizations taking place while they are leaving. Hollow cathode thrusters, which have a substantial potential difference across the baffle system, would be expected to have a smaller fraction of doubly ionized atoms for the same discharge voltage.

In order to calculate the backflow of neutrals into the ion chamber from the vacuum facility, a typical ion-gage reading of approximately 3×10^{-6} torr can be used. Most of the indicated reading should be due to propellant atoms during thruster operation, and the calibration factor (gage reading divided by actual pressure) is about 3 for mercury. A particle density of approximately 2×10^{16} per cubic meter would therefore be expected. A temperature of 300 K should be a conservative mean for the liquid-nitrogen-cooled tubes, the warmer baffles extending from these tubes, the room temperature end walls of the tank, and an ion-beam target that is warmer than room temperature. This density and temperature, together with an estimated effective backflow orifice area of 0.00196 square meter,[3] permit calculation of the backflow. This backflow, if singly ionized, is equivalent to only approximately 0.3 milliampere.

The theory of plasma probes and their use in ion thrusters has been adequately described in literature (refs. 21 and 41) and is repeated here only in summary form. The basic assumption generally used in analyzing ion-chamber probe data is that the electron distribution is composed of monoenergetic primaries superimposed on a Maxwellian background population. This assumption leads to primary and Maxwellian probe currents of

$$J_p = n_p qA\sqrt{\frac{2q\mathscr{E}_p}{m_e}}\,\frac{(1 + V/\mathscr{E}_p)}{4} \tag{28}$$

$$J_m = n_m qA\sqrt{qT_m/2\pi m_e}\,\exp(V/T_m) \tag{29}$$

where n_p and n_m are the densities of primary and Maxwellian electrons, q and m_e are the charge and mass of an electron, $\mathscr{E}_p$ and T_m are the energy of the primary electrons and temperature of Maxwellian electrons in eV, and V is the probe potential relative to the plasma potential in volts. The range of interest for the probe potential is $-\mathscr{E}_p \le V \le 0$. For the usual case of $\mathscr{E}_p \gg T_m$, a probe potential V approaching $-\mathscr{E}_p$ will yield only a linear variation of primary-electron current with probe potential (eq. (28)). This region of nearly linear variation is shown in the plot of sample probe data in figure 11(a) and is approximated by the dotted line. Note that the linear region

[3]An unpublished analysis by W. R. Kerslake indicated an effective flow factor of about 0.5 for the open area of a SERT II accelerator grid. The thruster used in this study had the same screen and accelerator grid thicknesses and hole diameters and thus should have the same flow factor. The accelerator open area was 50 percent of a 10-cm-diameter beam, so that this factor of 0.5 resulted in an effective sharp-edged orifice area of 0.00196 m^2.

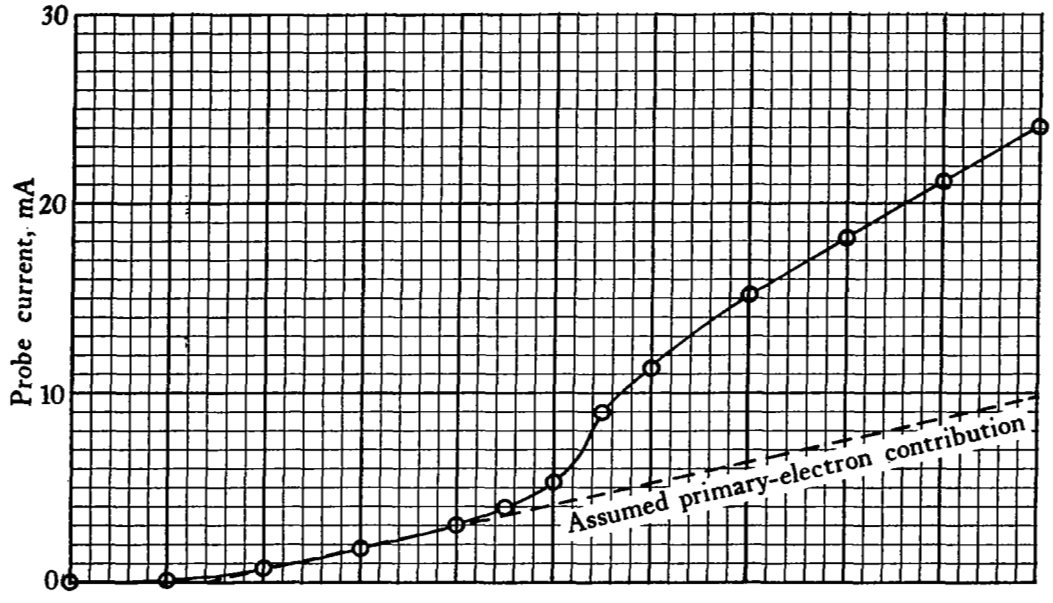

(a) Linear plot.

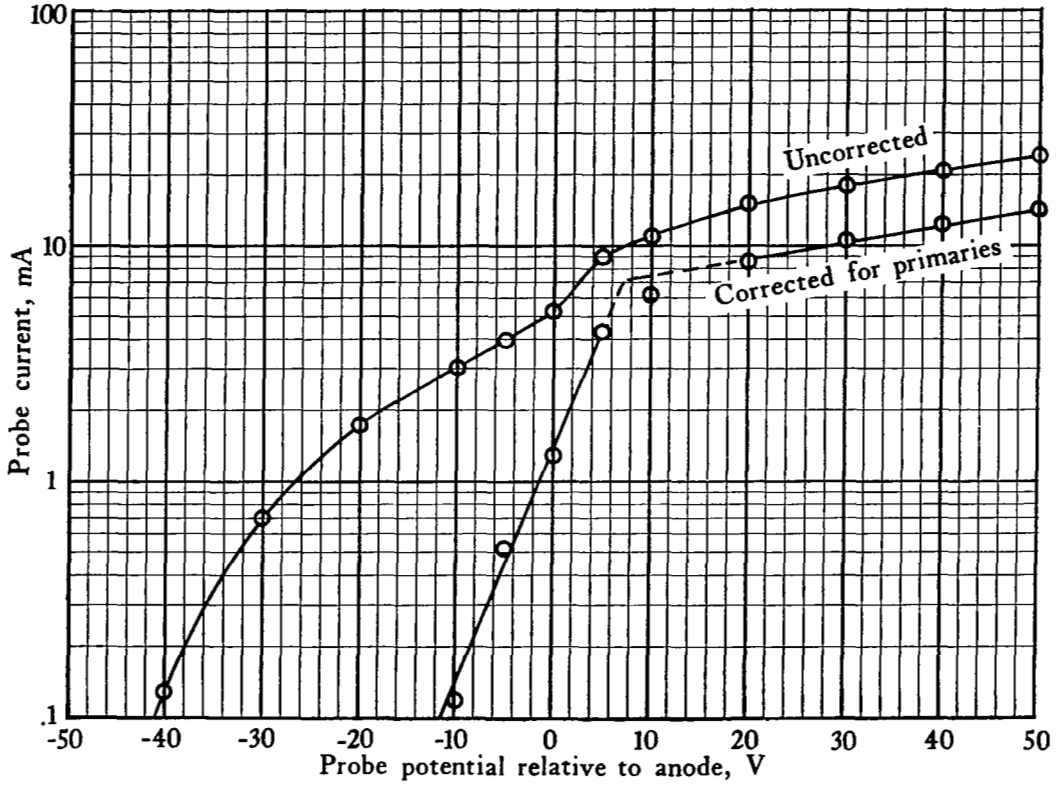

(b) Semilogarithmic plot.

Figure 11. - Typical Langmuir probe characteristics.

CS-58221

is actually somewhat curved. This curvature is due to the non-Maxwellian electrons actually having an energy distribution instead of being monoenergetic. The assumption of monoenergetic primaries, though, greatly simplifies the data analysis without departing from a reasonable approximation of the actual probe data. The contribution of the primaries (as approximated by the dotted line) can be subtracted from the measured probe currents to give a corrected current. The uncorrected and corrected probe currents are both shown in the semilogarithmic plot of figure 11(b). It is evident that the lower portion of the corrected curve closely approximates the straight line expected for a Maxwellian distribution. The upper portion of the corrected curve is ideally a horizontal line that indicates the plasma density, and the intersection of the two straight-line segments indicates the plasma potential. In practice, though, a probe potential above plasma potential leads to an enlarged plasma sheath around the probe, so that large positive voltages actually extract electrons from an area larger than the probe surface area. The plasma potential is ideally formed at the intersection of two precise straight-line segments. There is usually some noise in the ion chamber, and the superposition of curves that results while taking steady-state data is the reason customarily given for the rounding that occurs in this region (ref. 164).

RESULTS AND DISCUSSION

The ion-chamber performance data that were obtained without probes are presented first. Then, data for maximum propellant utilization are plotted and compared to the two theories presented earlier. Next, the ion-chamber probe data are presented and used to make a more detailed evaluation of the primary-electron-region approach to maximum propellant utilization. Last, a comparison is made with SERT-II throttling data.

Ion-Chamber Performance

The performance data for five basic ion-chamber configurations are shown in figure 12. Most of the data were obtained with a magnetic-field current of 1 ampere, as indicated earlier. Some of the data, though, were obtained at higher magnetic-field currents and are also included in figure 12. In addition, data for one configuration are included for operation with reverse feed, as opposed to the usual forward feed.

The shapes of the performance curves shown in figure 12 are typical of electron-bombardment thrusters. Each curve has a relatively flat portion below the "knee." The location of the knee and the nearly vertical portion above the knee depend on propellant flow rate. The curves of figure 12 can be used to show the relative importance of

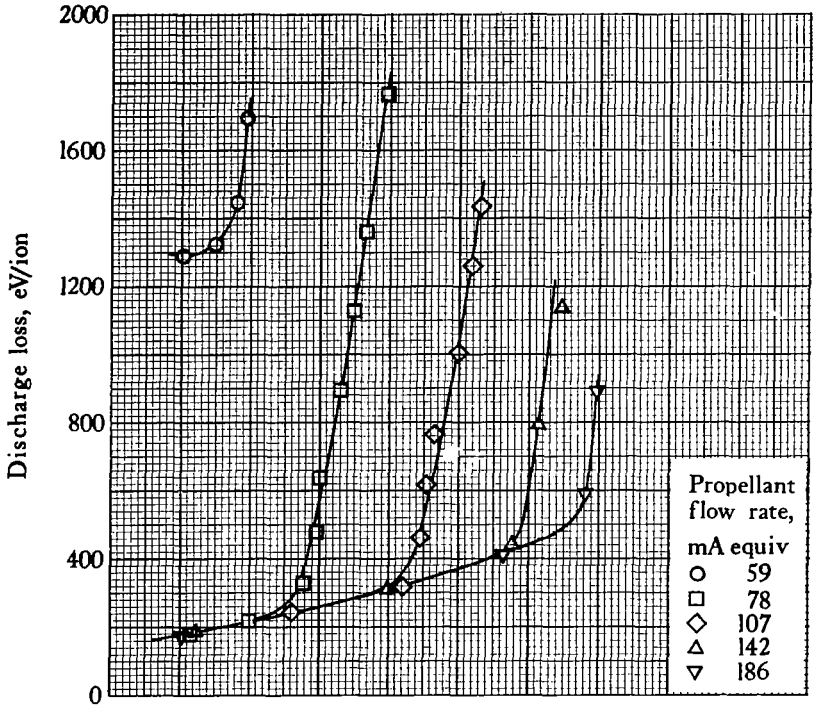

(a) Forward feed, 1-A magnet, 10-cm diameter, 7.2-cm length.

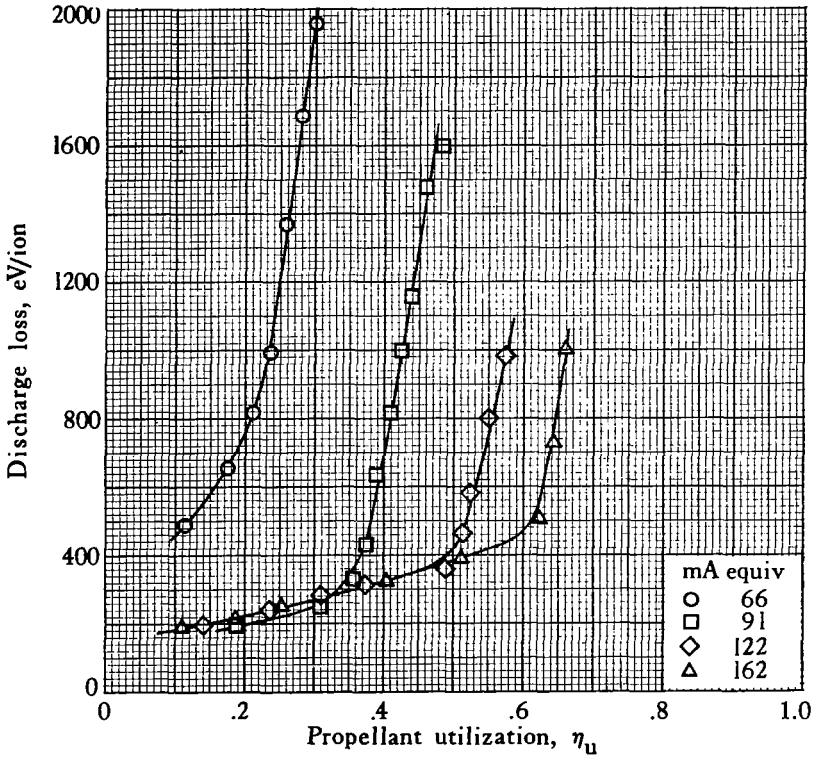

(b) Forward feed, 1-Amagnet, 10-cm diameter, 10.8-cm length.

Figure 12. - Ion-chamber performance.

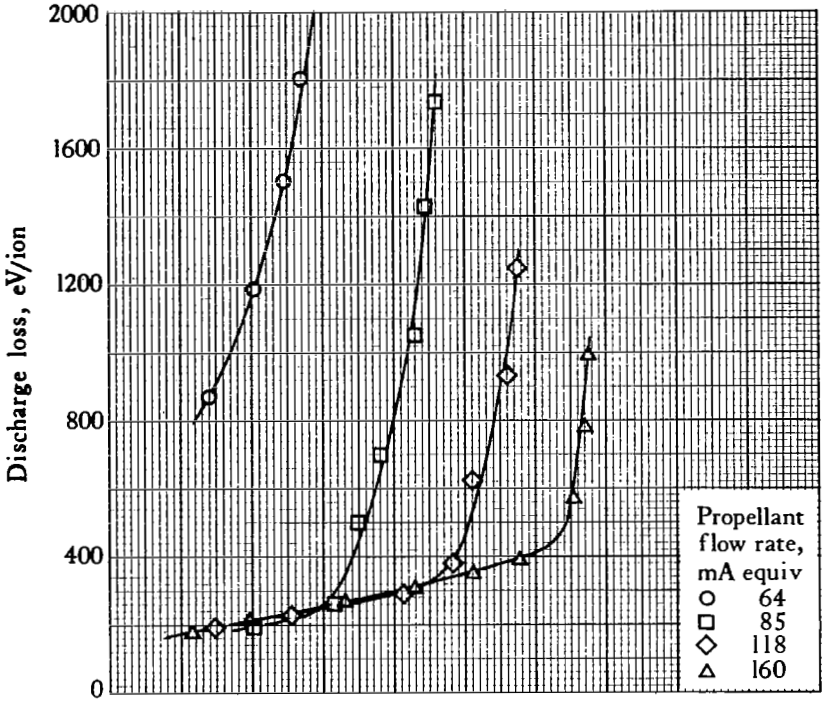

(c) Forward feed, 1-A magnet, 10-cm diameter, 14.4-cm length.

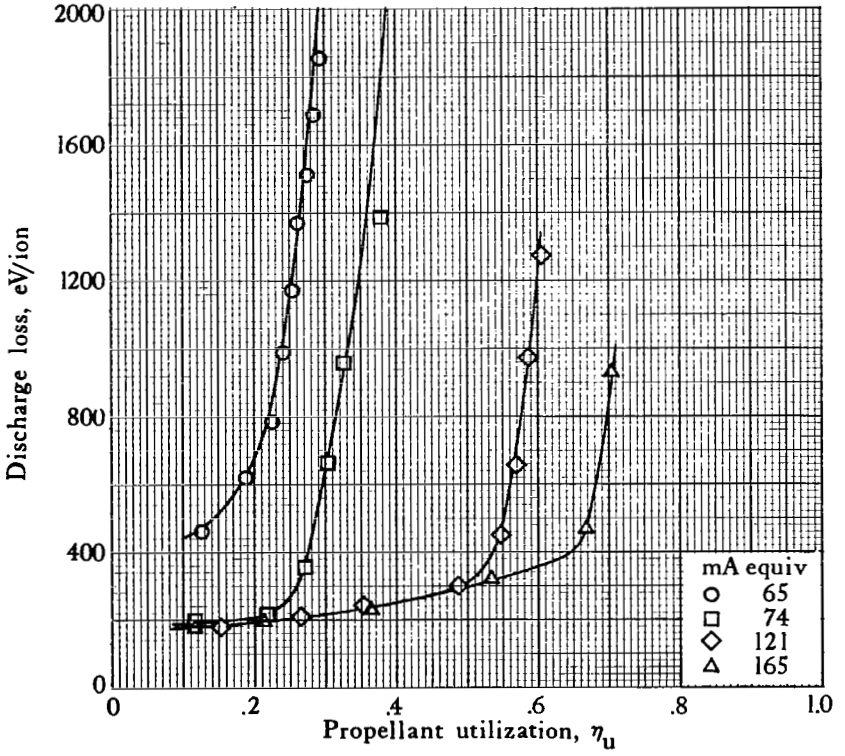

(d) Forward feed, 1-A magnet, 20-cm diameter, 9.4-cm length.

Figure 12. - Continued.

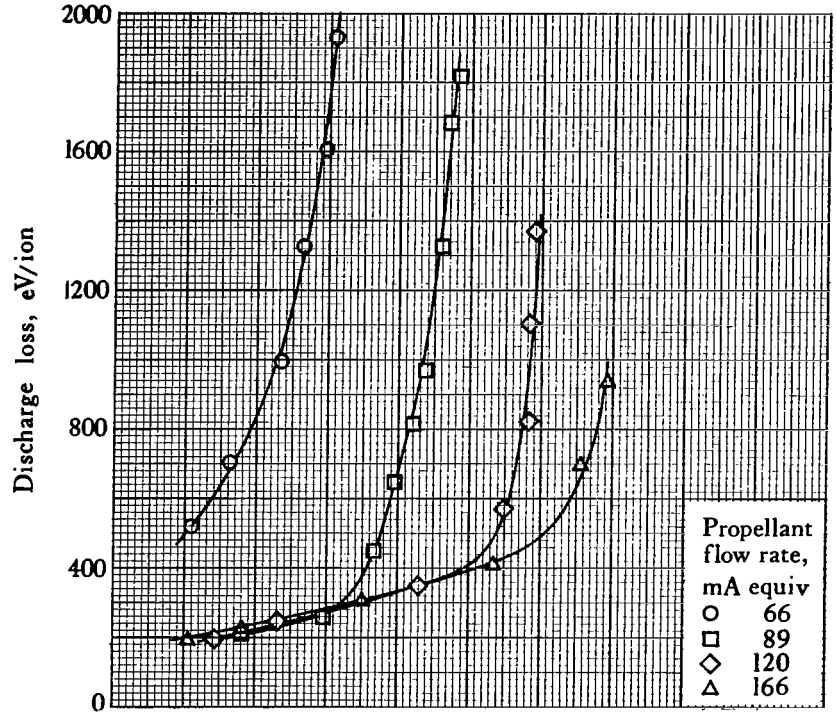

(e) Forward feed, 1-A magnet, 20-cm diameter, 14.4-cm length.

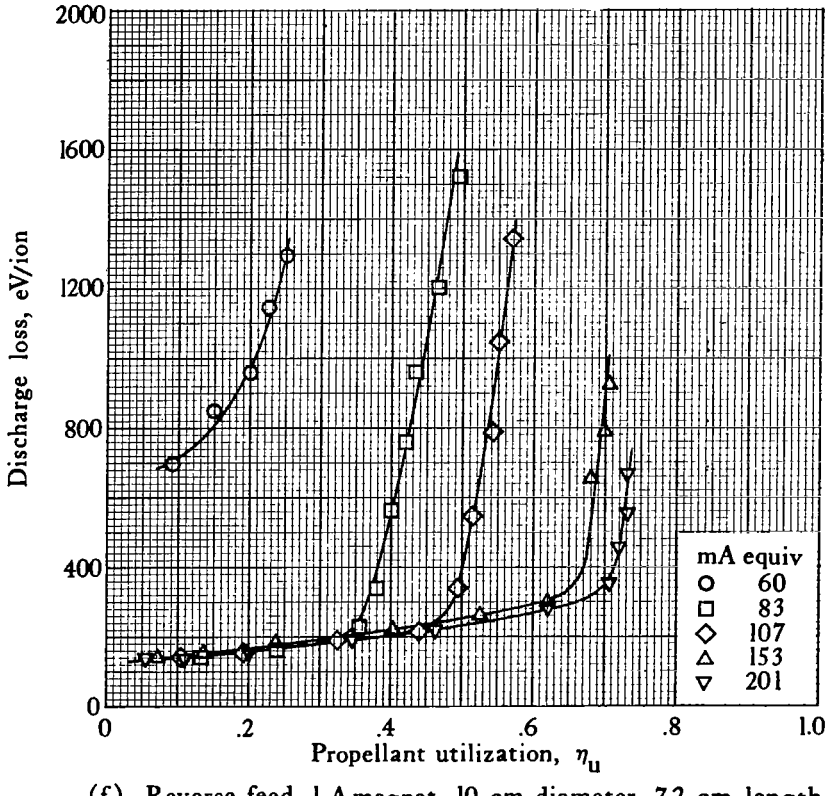

(f) Reverse feed, 1-A magnet, 10-cm diameter, 7.2-cm length.

Figure 12. - Continued.

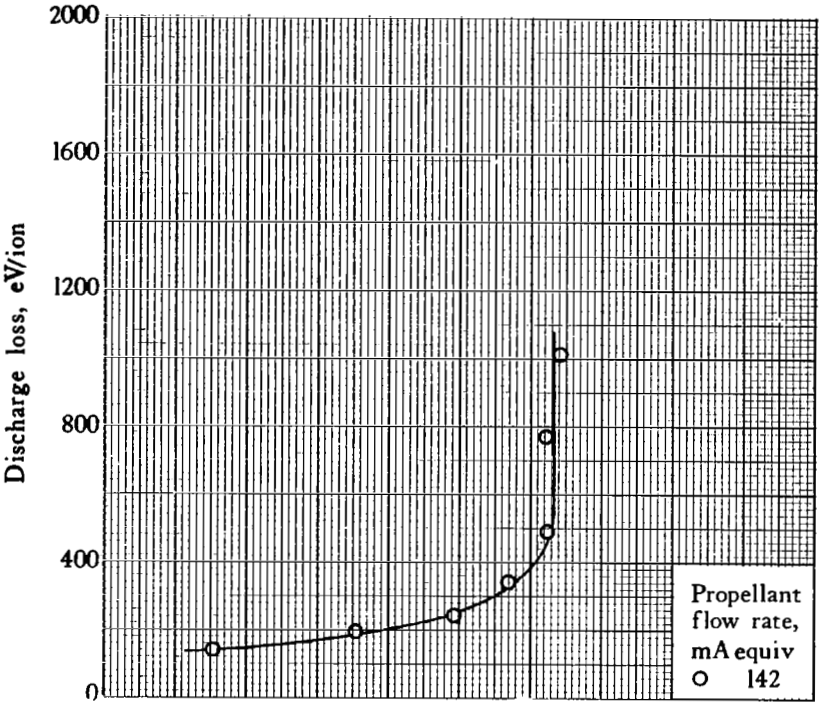

(g) Forward feed, 2-A magnet, 10-cm diameter, 7.2-cm length.

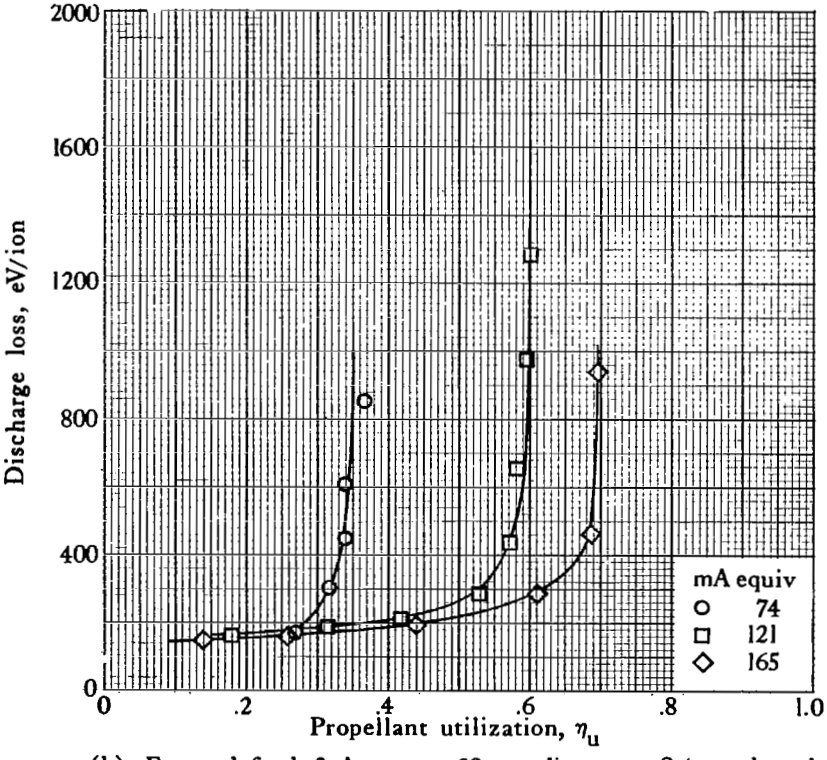

(h) Forward feed, 2-A magnet, 20-cm diameter, 9.4-cm length.

Figure 12. - Continued.

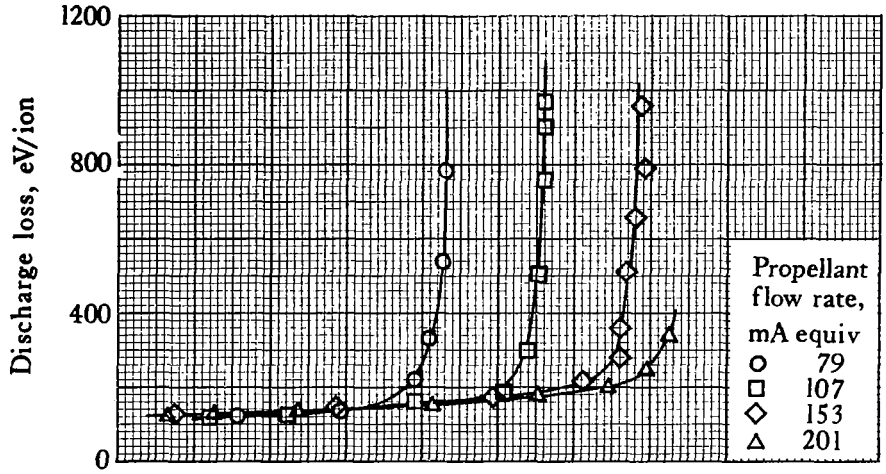

(i) Reverse feed, 2-A magnet, 10-cm diameter, 7.2-cm length.

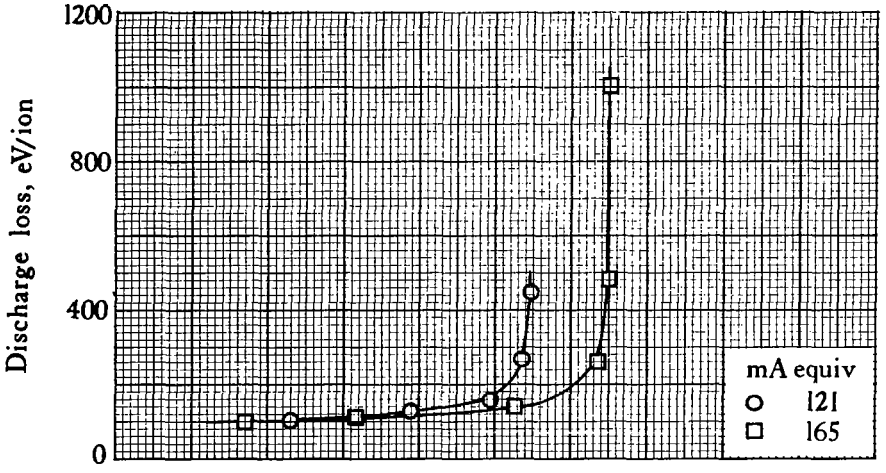

(j) Forward feed, 5-A magnet, 20-cm diameter, 9.4-cm length.

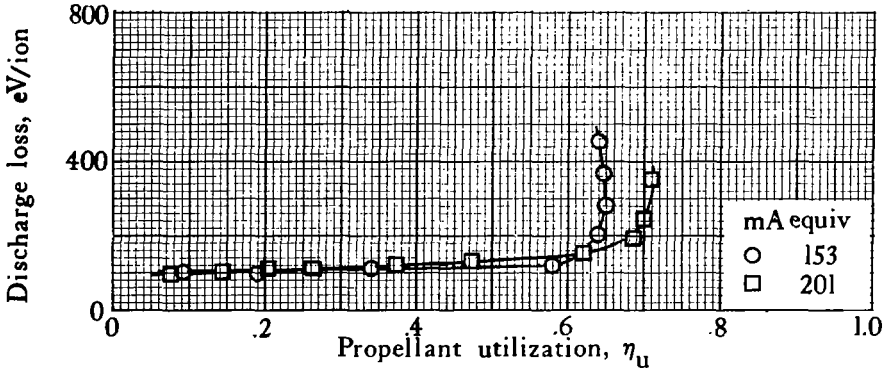

(k) Reverse feed, 5-A magnet, 10-cm diameter, 7.2-cm length.

Figure 12. - Concluded.

the various parameters that were varied. Comparisons of performance for the nearly vertical portions of the curves are adequately covered by subsequent parts of this section. Some comparison of the nearly horizontal portions below the "knee" is also of interest, however, and is covered here. Data for the five different configurations are plotted in figure 13. The neutral flows for these data are equivalent to a current range from 142 to 166 milliamperes (the current that would be measured if each propellant atom carried one electronic charge). This small variation has little effect on the performance below the knee, so that performance in this region can be compared directly. The variation between configurations is small below the knee - only some ±15 percent. In addition, there is no clear trend with ion-chamber volume or surface area. One can conclude that variations in ion-chamber configuration outside of the primary-electron region have no substantial effect on performance below the knee. Comments by Poeschel, Ward, and Knauer (ref. 113) indicate that knowledgeable workers in the ion-thruster field would expect such a result. Also, a ±15 percent variation can be sufficient to meet, or not meet, specific performance goals, and thus may appear quite important.

One might expect a discharge-loss sensitivity to changes in the primary-electron region. This expectation is borne out by the lower losses found at higher magnetic-field currents. The higher magnetic field decreases the losses, of course, by making it more difficult for the high-velocity primaries to reach the anode. The use of reverse feed gives a small further decrease in losses, presumably through a change towards a slightly more uniform distribution of ion production in the primary-electron region.

Double-valued ion-chamber performance data were not found, except possibly for a small region at high utilization with high magnetic-field currents. An intermittent short was found in the magnetic-field winding, and the extended double-valued performance data described in an earlier publication (ref. 136) were not encountered after this short was fixed.

Maximum Propellant Utilization

The widest range of operation was obtained at a magnetic-field current of 1 ampere. For this field current, though, no clear-cut maximum utilization was found (see figs. 12(a) to (f)). Instead, the utilization above the knee increased slowly with increasing losses. As a somewhat arbitrary choice, the utilization at an ion-chamber loss of 1000 eV per ion was used as a maximum. The use of some other high level of loss would have had no effect on the qualitative results presented and little effect on the quantitative results. Operation at higher magnetic-field strength gave nearly vertical lines for operation above the knee, so a similar arbitrary choice was not needed. For consistency, though, the same 1000-eV-per-ion definition was used.

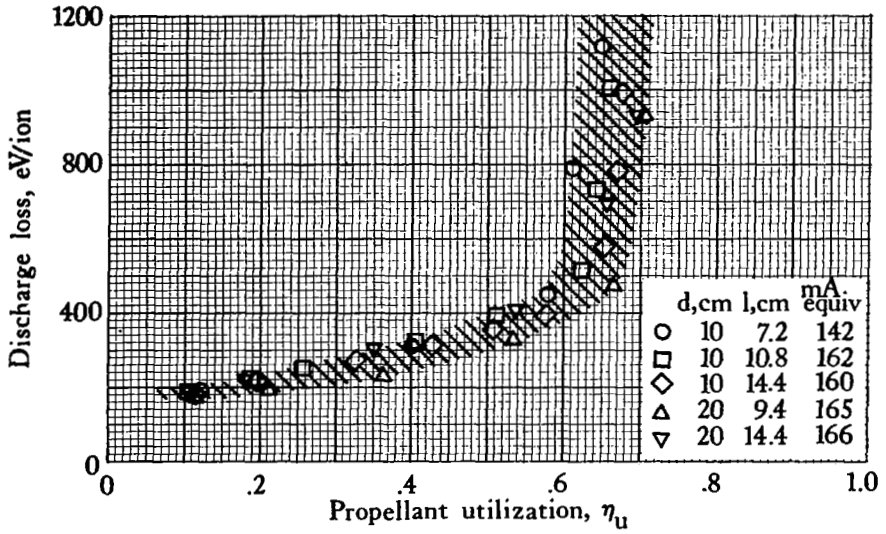

Figure 13. - Comparison of performance for different ion-chamber configurations. Forward feed, 1-A magnet.

CS-58214

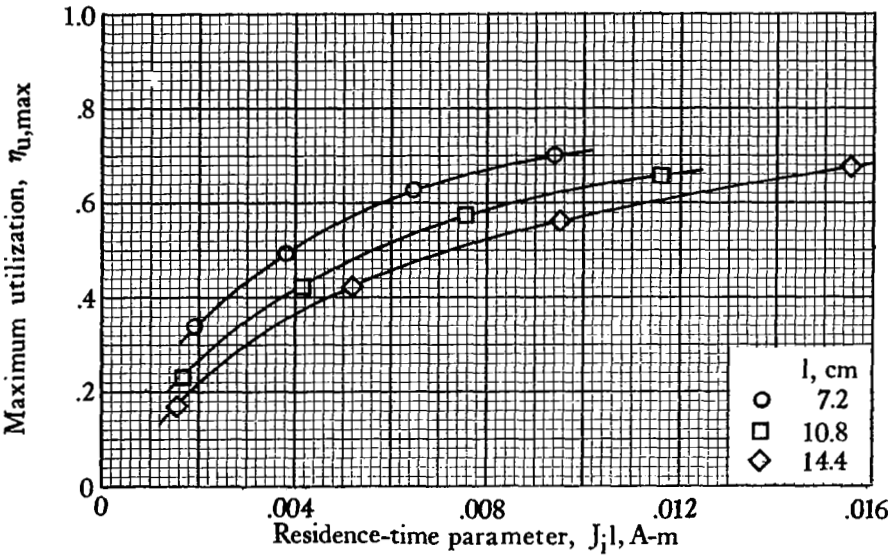

Figure 14. - Maximum-utilization data for 10-cm-diameter ion chambers plotted against residence-time parameter. Forward feed, 1-A magnet.

Having arrived at a definition of maximum utilization, it is now of interest to compare maximum-utilization data with the predictions of the previous analyses. Maximum-utilization data are plotted in figure 14 against the product $J_i l$ (ion-beam current times chamber length) for the three forward-feed 10-centimeter-diameter configurations at 1 ampere magnetic field. The product $J_i l$ is proportional to the residence-time correlation parameter $Kj_i l$ in equation (14). The data for the three configurations were not correlated by the parameter $J_i l$, inasmuch as the short-chamber data appear to be shifted to the left, and those of the long chamber shifted to the right. Indeed, for the data in figure 14, it is clear that J_i alone would have been a better correlation parameter than $J_i l$. This result should be expected for the highly divergent-field design used in these three configurations, where the primary-electron region is located close to the accelerator system. Older thruster designs, in which the primary-electron region extended the length of the ion chamber, were more suited to the residence-time approach.

Maximum-utilization data are plotted against total propellant mass flow in figure 15(a) for five forward-feed configurations operated at a magnetic-field current of 1 ampere. The un-ionized propellant mass flow was calculated for the data in figure 15(a) and plotted in figure 15(b). This calculation is defined by

$$J_o\Big|_{\text{un-ionized}} = (1 - \eta_{U,\,max})J_o\Big|_{\text{total}} \tag{30}$$

From figure 15(b), the maximum-utilization data correspond to a constant un-ionized loss rate equivalent to 52 milliamperes, ±8 percent. This result has considerably less scatter than the previously published maximum-utilization data (ref. 136). The reduced scatter is felt to be due to improved experimental techniques, particularly those techniques associated with the long time constants of the thruster used.

A difference between figure 15 and the results of the earlier portion of this investigation (ref. 136) is the agreement between data with 10- and 20-centimeter chamber diameters. There was poor agreement between data for these two diameters in the earlier results, and the lack of agreement was felt to be due to poor similarity for the region where primary electrons reach the anode. The short 10-centimeter-diameter section of the anode (in the 20-cm-diameter chamber) was only 0.6 centimeter long for the earlier data of the large chamber. This length was increased to 2.5 centimeters for the data presented in this report (see fig. 5) to assure a dimension greater than a primary-electron cyclotron radius. The close agreement of data for the two chamber diameters in figure 15 indicates the reasoning given earlier (ref. 136) for the poor correlation was probably correct.

The effects of a higher magnetic field and reverse feed of propellant are shown in the maximum-utilization data of figure 16. Reverse feed gave slightly higher maximum utilization of propellant, but again indicated a nearly constant loss of un-ionized propel-

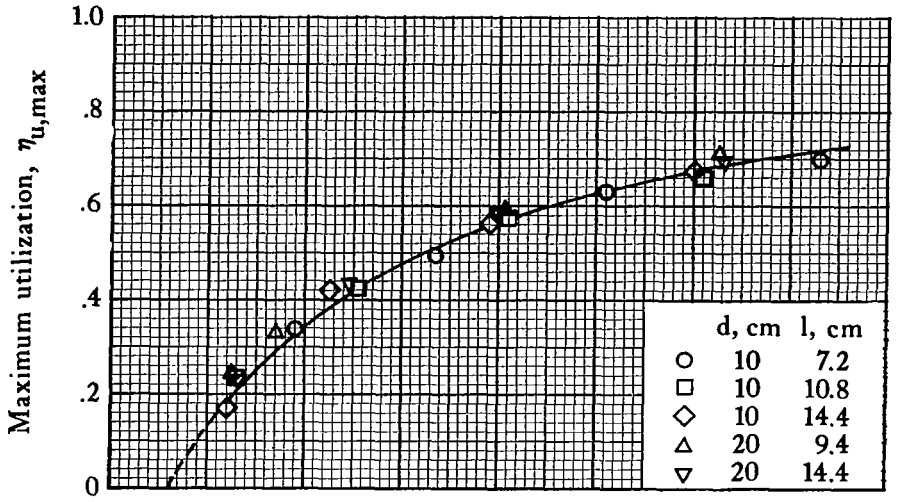

(a) Maximum propellant utilization.

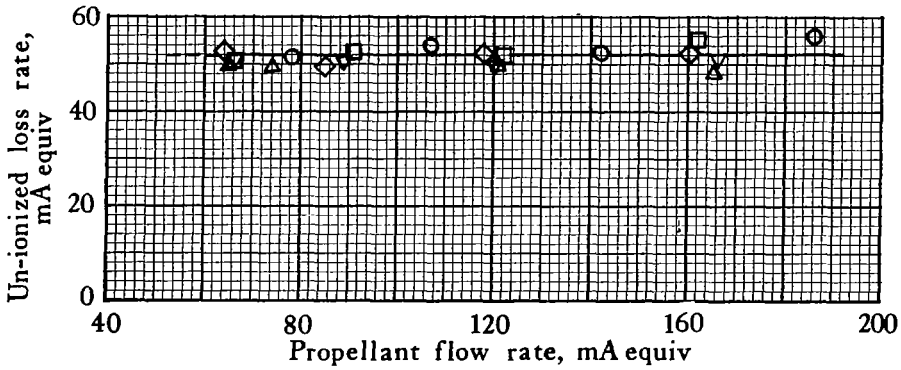

(b) Un-ionized propellant loss.

Figure 15. - Correlation of maximum utilization with total propellant flow rate. Forward feed, 1-A magnet.

lant, but again indicated a nearly constant loss of un-ionized propellant (about 6 to 14 percent lower than fig. 15). The data for the 2-ampere field current (forward feed) agreed more closely with the data shown in figure 15, but also showed a slightly lower loss of un-ionized propellant (0 to 10 percent lower).

The data for a magnet current of 5 amperes in figure 12 were not included in figure 15. At this high magnet current the discharge generally extinguished before a high emission could be reached. Also, a high impingement current was obtained well below the approximately 150-milliampere limit for lower magnet currents. This latter condition indicated a beam-current profile that was more peaked, presumably because the discharge was concentrated nearer the ion-chamber axis by the high magnetic field.

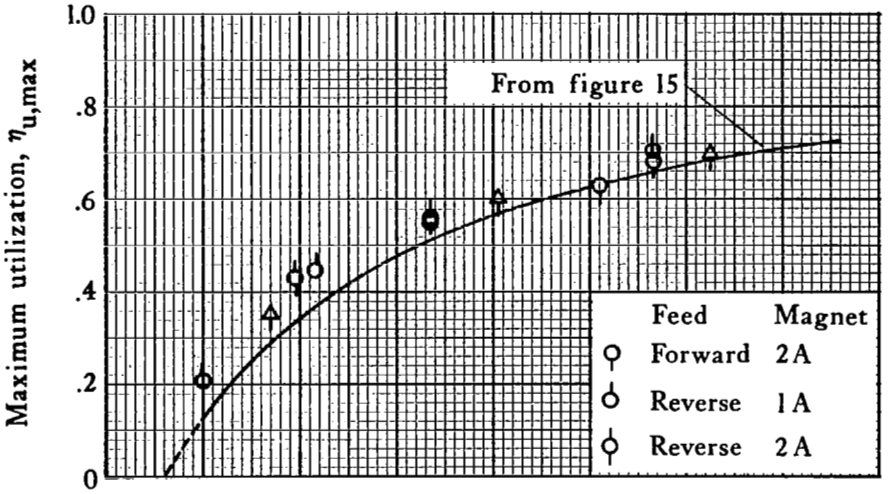

(a) Maximum propellant utilization.

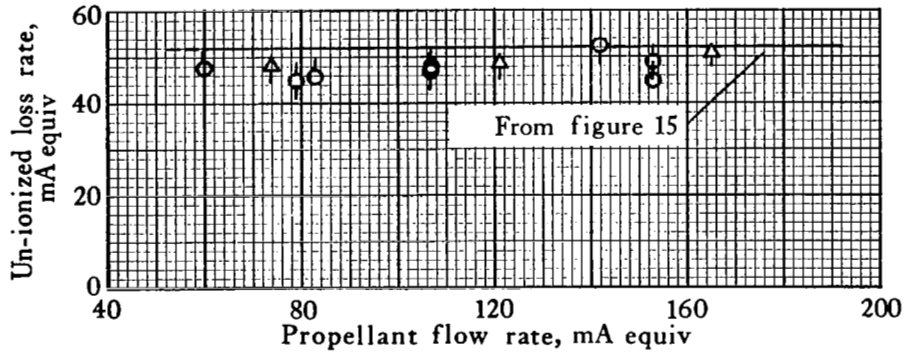

(b) Un-ionized propellant loss.

Figure 16. - Effect of feed and magnet current on correlation. Symbols same as figure 15, except for additions noted.

As a general conclusion, then, a highly divergent-field thruster shows a nearly constant loss of un-ionized propellant at maximum utilization. This result can be obtained from either equation (20) or equation (26) with the proper selection of constants. In agreement with either of these equations of the primary-electron-region approach, the changes outside of the primary-electron region have no significant effect on the loss of un-ionized propellant. Further, even changes that do affect the primary-electron region can have a small effect on this value of propellant loss if the magnetic-field shape is constant (which is substantially true of the 1- to 2-ampere range included in figs. 15 and 16).

Ion-Chamber Probe Data

Thorough Langmuir-probe surveys have been made of current divergent-field ion-chamber designs at certain selected operating conditions (refs. 97 and 113). The objective in obtaining the probe data of this investigation was not to duplicate the published ion-chamber surveys. Instead, the objective was to take a few selected probe locations and obtain data for a wide range of propellant flow rates and ion-chamber configurations. Probe A (fig. 7) was selected as a representative sample of the primary-electron region. Probe B was located on the "critical field line" that separates the primary-electron region from the rest of the chamber. (The name "critical field line" was apparently first used by King, Poeschel, and Ward, ref. 119.) Probe C was selected as a representative sample of the ion chamber outside of the primary-electron region.

The ion-chamber probe data were obtained at several emission currents for each of several mass flows. Typical data from probe A are shown in figure 17 for one propellant mass flow. The density of Maxwellian electrons first increased with discharge, reached a maximum near the "knee" of the curve for ion-beam current, and then slowly decreased at higher discharge currents. The ratio of primary to Maxwellian electron densities increased continuously with discharge current throughout the range investigated. The electron temperature also increased with discharge current, but much less rapidly.

The probe data were cross plotted to determine ion-chamber parameters for 1000-eV-per-ion condition defined as maximum propellant utilization. For the data in figure 17 the value of 1000 eV per ion is reached at a discharge current of about 2.1 amperes. These cross-plotted values are presented in figure 18. The scatter in the data of figure 18 is to a large extent a measure of the uncertainties involved in obtaining and analyzing ion-chamber probe data. The overall uncertainty was estimated by Strickfaden and Geiler (ref. 21) as being about 30 percent, with most of the error associated with the straight-line assumption of primary-electron contribution. The frequent replacement of probes was necessary because of cathode sputtering and no doubt added to the total scatter. This sputtering problem could have been avoided by using a hollow or oxide cathode. A hollow cathode would have introduced a perturbation in neutral density and thus analytical uncertainty. An oxide cathode would be likely to affect utilization measurements at very high discharge losses through evaporation from ion bombardment.

The temperature of the Maxwellian electrons in the primary-electron region (probe A, fig. 18(a)) averaged about 5 eV, which agrees closely with values obtained previously at lower utilizations (ref. 123). This temperature drops slightly to about 4 eV at the critical field line and is only about 2.5 eV outside the primary-electron region.

The ratio of primary-to-Maxwellian electron densities averages about 0.4 for the primary-electron region (probe A, fig. 18(b)). This ratio drops to about 0.1 for the critical field line. Similar data are not shown for the ion chamber outside the primary-

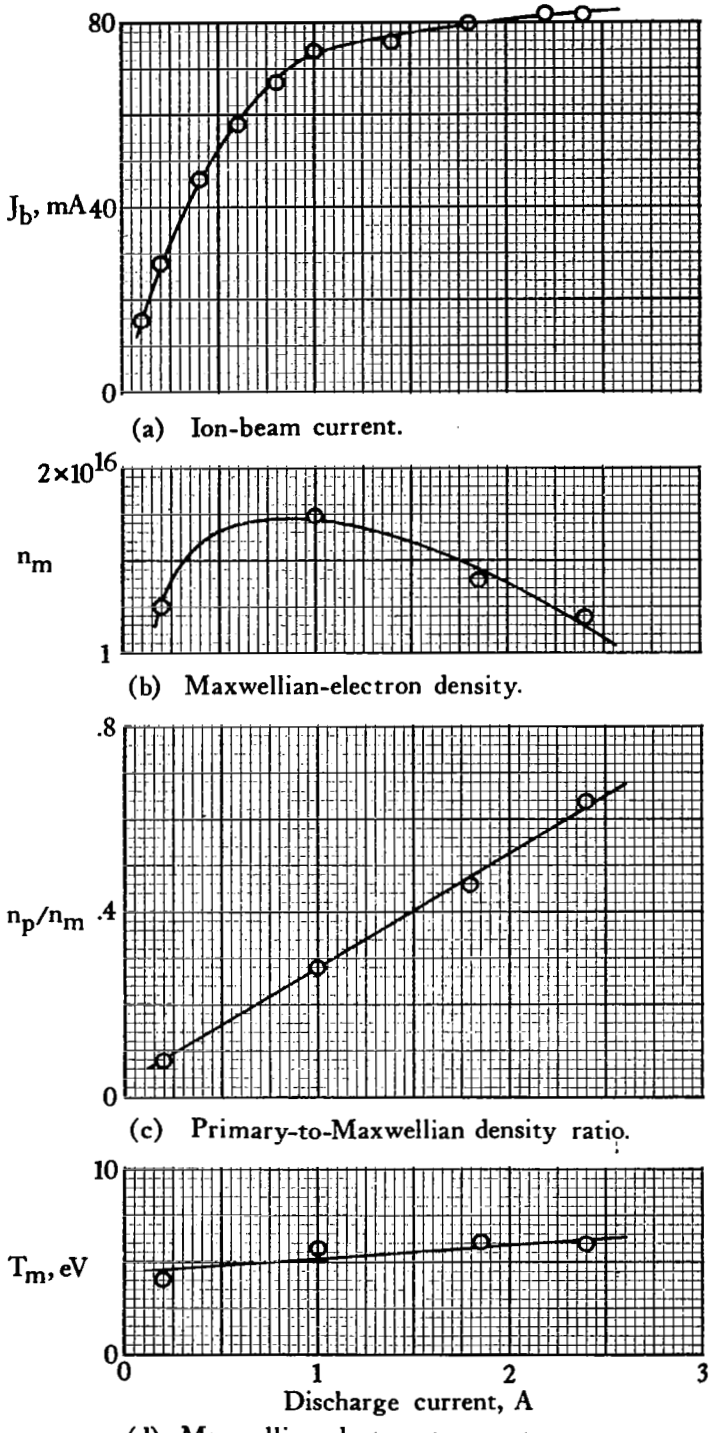

Figure 17. - Typical variation of performance and probe data with discharge (anode) current. Probe A, 131 mA equiv.

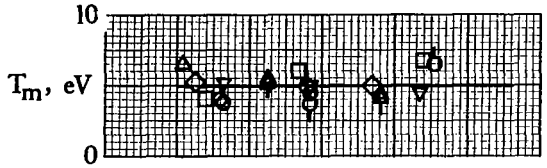

(a) Maxwellian-electron temperature, probe A.

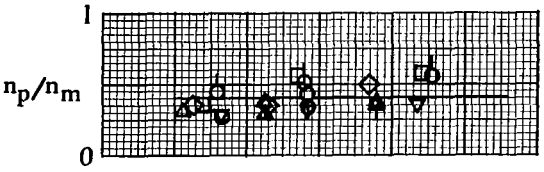

(b) Primary-to-Maxwellian density ratio, probe A.

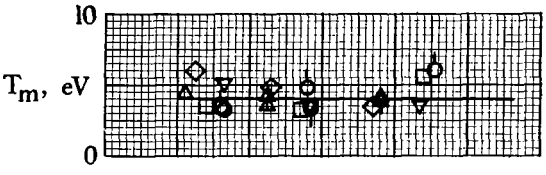

(c) Maxwellian-electron temperature, probe B.

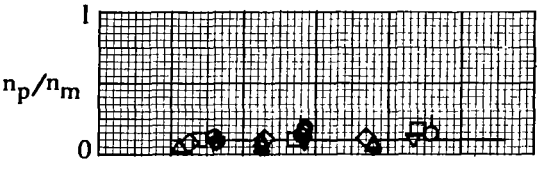

(d) Primary-to-Maxwellian density ratio, probe B.

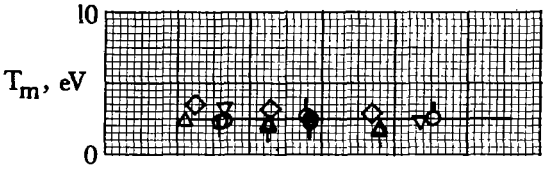

(e) Maxwellian-electron temperature, probe C.

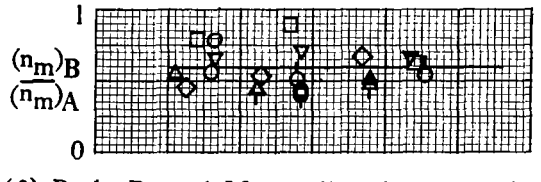

(f) Probe B-to-A Maxwellian density ratio.

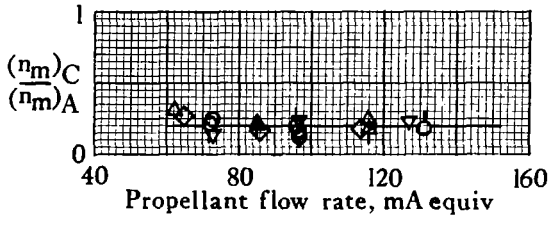

(g) Probe C-to-A Maxwellian density ratio.

Figure 18. - Ion-chamber probe data for maximum utilization. Symbols same as figures 15 and 16.

electron region (probe C) because the ratio was too low to measure accurately ($\leq$0.02). It should be noted that the primary-to-Maxwellian density ratio in the primary-electron region is well above the $\leq$0.1 value found previously at more normal operating conditions. This high value is no doubt due to the 1000-eV-per-ion discharge losses associated with figure 18. One should also note that the electron parameters for this high discharge loss indicate that most of the ionization will take place in the primary-electron region, as assumed in the analysis. The mean energy of the primary electrons ranged from about 35 to 40 eV at probe A, ranged from 30 to 35 eV at probe B, and was less than 30 eV at probe C.

The data shown in figure 18 show no significant trends with propellant mass flow or ion-chamber surface area. The use of the constant values of 5 eV for Maxwellian-electron temperature and 0.4 for primary-to-Maxwellian density ratio appears justified for the primary-electron region values of equation (26).[4] These values, together with a value of 0.011 meter for V_p/A_p (which can be obtained from a magnetic-field map such as shown in fig. 3), give a neutral density of 3.11×10^{18} per cubic meter. This neutral density, equation (4), an equivalent sharp-edged orifice area of 0.00196 square meter, and an assumed wall temperature of 500 K result in a neutral loss rate equivalent to 56 milliamperes. This value is quite close to the experimentally determined value of 52 milliamperes (fig. 15). This close agreement is well within the possible error of the analytical model and constitutes an independent check on the analytical model.

Comparison With SERT II Data

It is of interest to compare the results of this investigation with published data. Probably the most documented thruster of divergent-field design is the one used on the SERT II flight (ref. 110). The SERT II throttling data (ref. 109) were reviewed and found to show the same nearly constant loss rate for un-ionized propellant that was found in this investigation. The comparison was not possible for the full throttling range above 250 eV per ion. But this value was high enough to be in the "knee" of the loss curve and thus be substantially proportional to maximum utilization as defined in this report. The un-ionized propellant loss was equivalent to a current range from 45 to 50 milliamperes for 250 eV per ion and a total propellant flow range of 2.5 to 1. (In a private communication with Byers has stated that fig. 6(b) of ref. 109 is incorrect. The utilization at 250 eV/ion and a beam current of 0.20 was close to 0.80.) The level of un-ionized pro-

[4]The temperature enters as a square root in eq. (26), so that the possible variation of temperature indicated by fig. 18(a) would enter as less than a linear effect. In a similar manner, the possible variation of primary-to-Maxwellian density ratio would have less than a linear effect over the range of interest (see fig. 4).

pellant loss rate predicted from the theory of this investigation, however, was substantially above the observed equivalent range of 45 to 50 milliamperes. An unusual aspect of SERT II ion-chamber operation (with the accelerator system used for the throttling data, ref. 109) was for formation of several-volt ridges in plasma potential near the anode (refs. 85 and 113). Although the cause of these potential ridges is not clear, their presence probably reduced radial ion losses in their vicinity. If one neglects the boundary area of the primary-electron region near these ridges, the calculated neutral loss becomes much closer to the experimental values. Also, the introduction of propellant through the hollow cathode (about one-third of the total propellant flow at SERT II design conditions) was a departure from the uniform conditions assumed for the theory derivation. Thus, although SERT II data are in good qualitative agreement with the theory of this investigation, it is apparently possible to obtain special plasma conditions that will affect the quantitative agreement of experimental data with the theory presented in this report. There is no evidence for reduced radial ion loss in the present investigation, inasmuch as probes A and B had an average potential difference of less than 1 volt.

CONCLUDING REMARKS

The most significant results of this investigation are the analyses of maximum propellant utilization and the experimental agreement that was obtained with these analyses. The significance of these results is in the implied ability to predict maximum utilization of new designs from the field shape, and the inverse ability to select field shapes that should give high utilization.

The results of this investigation can be expressed simply: the loss rate of un-ionized propellant at maximum utilization is nearly a constant over a wide range of total propellant flow rate. The simplicity of this result permits rapid prediction of total flow-rate effects from operation at one total flow rate.

In addition to the general design application, the results of this investigation are particularly significant for throttled operation of a fixed-configuration thruster. Because of variations in available power, many missions require considerable operation at less than maximum thrust. Further, to avoid either large power losses or large propellant losses, such part-thrust operation should be near the "knee" of the ion-chamber loss curve. This knee will shift substantially in the same manner as maximum propellant utilization. Inasmuch as the un-ionized-propellant loss rate will be a larger fraction of total flow rate at part-throttle operation, one can expect the most difficult requirement for utilization to be at the lowest thrust level to be used. Without any configuration changes accompanying thrust reduction, then, a thruster with good part-thrust perform-

ance would be expected to have very high utilization at full thrust. Good qualitative agreement of these results was found with published SERT II throttling data.

Lewis Research Center,
National Aeronautics and Space Administration,
Cleveland, Ohio, September 17, 1971,
113-26.

REFERENCES

1. Kaufman, Harold R.; and Reader, Paul D.: Experimental Performance of Ion Rockets Employing Electron-Bombardment Ion Sources. Paper 1374-60, ARS, Nov. 1960.
2. Kaufman, Harold R.: An Ion Rocket with an Electron-Bombardment Ion Source. NASA TN D-585, 1961.
3. Phillips, C. E. W.: The Action of Magnetized Electrodes upon Electrical Discharge Phenomena in Rarefied Gases. Preliminary Note. Proc. Roy. Soc. (London), Ser. A, vol. 64, 1898, pp. 172-176.
4. Livingston, M. Stanley; Holloway, M. G.; and Baker, C. P.: Cyclotron. Rev. Sci. Instr., vol. 10, no. 2, Feb. 1939, pp. 63-67.
5. Finkelstein, A. Theodore: A High Efficiency Ion Source. Rev. Sci. Instr., vol. 11, no. 3, Mar. 1940, pp. 94-97.
6. Backus, J.: Theory and Operation of a Philips Ionization Gauge Type Discharge. The Characteristics of Electrical Discharges in Magnetic Fields. A. Guthrie and R. K. Wakerling, eds., McGraw-Hill Book Co., Inc., 1949, pp. 345-369.
7. Guthrie, A.; and Wakerling, R. K., eds.: Sources and Collectors for Use in Calutrons. Radiation Laboratory, Univ. California (AEC Rep. TID-5218), June 1949.
8. Von Ardenne, Manfred: New Developments in Applied Ion and Nuclear Physics. Rep. AERE-LIB/TRANS-758, Atomic Energy Research Establishment, 1957.
9. Meyerand, Russell G., Jr.; and Brown, Sanborn C.: High-Current Ion Source. Rev. Sci. Instr., vol. 30, no. 2, Feb. 1959, pp. 110-111.
10. Moak, C. D.; Banta, H. E.; Thurston, J. N.; Johnson, J. W.; and King, R. F.: Duo Plasmatron Ion Source for Use in Accelerators. Rev. Sci. Instr., vol. 30, no. 8, Aug. 1959, pp. 694-699.

11. Langmuir, David B.; and Stuhlinger, E., eds.: Electricstatic Propulsion. Vol. 5 of Progress in Astronautics and Aeronautics. Academic Press, 1961.

12. Reader, Paul D.: Investigation of a 10-Centimeter-Diameter Electron-Bombardment Ion Rocket. NASA TN D-1163, 1962.

13. Kerslake, William R.: Accelerator Grid Tests on an Electron-Bombardment Ion Rocket. NASA TN D-1168, 1962.

14. Reader, Paul D.: Scale Effects on Ion Rocket Performance. ARS J., vol. 32, no. 5, May 1962, pp. 711-714.

15. Pawlik, Eugene V.; and Wenger, Norman C.: Performance Evaluation of a Mercury-Propellant Feed System for a Flight-Model Ion Engine. NASA TN D-1213, 1962.

16. Milder, Nelson L.: Comparative Measurements on Singly and Doubly Ionized Mercury Produced by an Electron-Bombardment Ion Engine. NASA TN D-1219, 1962.

17. Reader, Paul D.; and Finke, Robert C.: An Electron-Bombardment Ion Rocket Operated on Alternating-Current Supplies. NASA TN D-1457, 1962.

18. King, Harry J.; and Kohlberg, Ira: Low Current Density Ion Engine Development. Rep. 38-TR-102, Ion Physics Corp. (NASA CR-52440), Jan. 1963.

19. Kohlberg, Ira: Analytic Considerations Related to the Lewis Type Bombardment Ion Engine. Paper 63-030B, AIAA, Mar. 1963.

20. Stover, John B.: Electric Breakdown and Arcing in Experimental Ion Thrustor Systems. Paper 63-057, AIAA, Mar. 1963.

21. Strickfaden, William B.; and Geiler, Kenneth L.: Probe Measurements of the Discharge in an Operating Electron Bombardment Engine. Paper 63-056, AIAA, Mar. 1963.

22. Kerslake, William R.: Charge-Exchange Effects of the Accelerator Impingement of an Electron-Bombardment Ion Rocket. NASA TN D-1657, 1963.

23. Kemp, Robert F.; Sellen, J. M., Jr.; and Pawlik, Eugene V.: Neutralizer Tests on a Flight-Model Electron-Bombardment Ion Thrustor. NASA TN D-1733, 1963.

24. King, H. J.; and Quintal, B. S.: Lewis Type Bombardment Ion Engine: d. c. and Pulsed Operation. AIAA J., vol. 1, no. 11, Nov. 1963, pp. 2661-2663.

25. Kerslake, William R.; and Pawlik, Eugene V.: Additional Studies of Screen and Accelerator Grids for Electron-Bombardment Ion Thrustors. NASA TN D-1411, 1963.

26. Reader, Paul D.: Ion Rocket with a Permanent Magnet. Astronautics and Aerospace Eng., vol. 1, no. 9, Oct. 1963, p. 83.

27. Hyman, J., Jr.; Eckhardt, W. O.; Knechtli, R. C.; and Buckey, C. R.: Formation of Ion Beams from Plasma Sources. I. AIAA J., vol. 2, no. 10, Oct. 1964, pp. 1739-1748.

28. Nakanishi, Shigeo; Pawlik, Eugene V.; and Baur, Charles W.: Experimental Evaluation of Steady-State Control Properties of an Electron-Bombardment Ion Thrustor. NASA TN D-2171, 1964.

29. Milder, Nelson L.; and Kerslake, William R.: Evaluation of Filament Deterioration in Electron-Bombardment Ion Sources. NASA TN D-2173, 1964.

30. Reader, Paul D.; and Mickelsen, William R.: Ion Propulsion Systems for Spacecraft. J. Spacecraft Rockets, vol. 2, no. 4, July-Aug. 1965, pp. 577-583.

31. Kerslake, William R.: Cathode Durability in the Mercury Electron-Bombardment Ion Thrustor. Paper 64-683, AIAA, Aug. 1964.

32. Reader, Paul D.: Experimental Performance of a 50 Centimeter Diameter Electron-Bombardment Ion Rocket. Paper 64-689, AIAA, Aug. 1964.

33. Stover, John B.: Effect of Thrustor Arcing on Ion Rocket System Design. Paper 64-682, AIAA, Aug. 1964.

34. Nakanishi, S.; and Pawlik, E. V.: Preliminary Experimental Operation of High-Voltage Isolation Device for Propellant System of an Ion Rocket. NASA TM X-1026, 1964.

35. Pawlik, Eugene V.; and Nakanishi, Shigeo: Experimental Evaluation of Size Effects on Steady-State Control Properties of Electron-Bombardment Ion Thrustor. NASA TN D-2470, 1964.

36. Pawlik, Eugene V.: An Experimental Evaluation of Array of Three Electron-Bombardment Ion Thrustors. NASA TN D-2597, 1965.

37. Reader, Paul D.: Experimental Effects of Propellant-Introduction Mode on Electron-Bombardment Ion Rocket Performance. NASA TN D-2587, 1965.

38. Cole, Robert K.; Hall, David F.; Kemp, Robert F.; and Sellen, J. M., Jr.: Ion Beam Neutral Component Determination by Resonance Radiation Absorption. AIAA J., vol. 3, no. 2, Feb. 1965, pp. 263-269.

39. Cybulski, Ronald J.; Shellhammer, Daniel M.; Lovell, Robert R.; Domino, Edward J.; and Kotnik, Joseph T.: Results from SERT I Ion Rocket Flight Test. NASA TN D-2718, 1965.

40. Pawlik, Eugene V.; Margosian, Paul M.; and Staggs, John F.: A Technique for Obtaining Plasma-Sheath Configurations and Ion Optics for an Electron-Bombardment Ion Thrustor. NASA TN D-2804, 1965.

41. Kerrisk, Daniel J.; and Masek, T. D.: Plasma Nonuniformity on Grid Erosion in an Electron Bombardment Ion Engine. AIAA J., vol. 3, no. 6, June 1965, pp. 1060-1066.

42. Kerslake, William R.: Preliminary Operation of Oxide-Coated Brush Cathodes in Electron-Bombardment Ion Thrustors. NASA TM X-1105, 1965.

43. Kaufman, Harold R.: Performance Correlation for Electron-Bombardment Ion Sources. NASA TN D-3041, 1965.

44. Kohlberg, I.; and Nablo, S.: Physical Phenomena in Bombardment Ion Sources. Physics and Technology of Ion Motors. Frank E. Marble and Jean Surugue, eds., AGARDograph 88, Gordon and Breach Science Publ., 1966, pp. 156-206.

45. Sellen, J. M., Jr.; and Kemp, Robert F.: Research on Ion Beam Diagnostics. Rep. TRW-4381-6017-R0-000, TRW Systems (NASA CR-54692), Feb. 10, 1966.

46. Kerrisk, Daniel J.; and Masek, Tommy D.: A Zero Gravity Mercury Propellant Feed System. Paper 66-250, AIAA, Mar. 1966.

47. Knauer, W.; Hagen, G.; Gallagher, H.; and Stack, E.: Investigation of the Discharge in Electron Bombardment Thrustors. Paper 66-244, AIAA, Mar. 1966.

48. Reader, Paul D.: Durability Tests of Mercury Electron-Bombardment Ion Thrustors. Paper 66-231, AIAA, Mar. 1966.

49. Nakanishi, Shigeo: Experimental Investigation of a High-Voltage Isolation Device for Ion-Thrustor Propellant Feed. NASA TN D-3535, 1966.

50. Wasserbauer, Joseph F.: A 5-Centimeter-Diameter Electron-Bombardment Thrustor with Permanent Magnets. NASA TN D-3628, 1966.

51. Cohen, Allan J.: Onset of Anomalous Diffusion in Electron-Bombardment Ion Thrustor. NASA TN D-3731, 1966.

52. Shaw, E. K.: One- and Two-Dimensional Steady-State Low Pressure Discharge Theory. Rep. ML-1495, Stanford Univ. (NASA CR-54665), 1967.

53. Kerslake, William R.: Oxide-Cathode Durability in the Mercury Electron-Bombardment Ion Thrustor. NASA TN D-3818, 1967.

54. Margosian, Paul M.: Preliminary Tests of Insulated Accelerator Grid for Electron-Bombardment Thrustor. NASA TM X-1342, 1967.

55. Kerslake, William R.; Wasserbauer, Joseph F.; and Margosian, Paul M.: Experimental Mercury Bombardment Thruster at Submillipound Thrust. AIAA J., vol. 5, no. 4, Apr. 1967, pp. 683-691.

56. King, H. J.; Eckhardt, W. O.; Ward, J. W.; and Knechtli, R. C.: Electron-Bombardment Thrusters Using Liquid-Mercury Cathodes. J. Spacecraft Rockets, vol. 4, no. 5, May 1967, pp. 599-602.

57. King, H. J.; Molitor, J. H.; Kovar, D. G.; and Muldoon, W. J.: Development and Testing of a Lightweight Flight Prototype Ion Engine System. J. Spacecraft Rockets, vol. 4, no. 5, May 1967, pp. 603-609.

58. Margosian, Paul M.; and Kerslake, William R.: Experimental Evaluation of a Two-Directional Electron-Bombardment Ion Thruster. AIAA J., vol. 5, no. 5, May 1967, pp. 833-839.

59. Hodgson, Rodney T.; Fitzgerald, Dennis C.; and Mickelsen, William R.: Fundamental Plasma Processes in Electron-Bombardment-Thruster Ionization Chambers. Advanced Electric Propulsion Research. Rep. 5, Colorado State Univ. (NASA CR-88419), July 1967.

60. Kerrisk, D. J.; and Kaufman, H. R.: Electric Propulsion Systems for Primary Spacecraft Propulsion. Paper 67-424, AIAA, July 1967.

61. Pawlik, Eugene V.; and Reader, Paul D.: Accelerator Grid Durability Tests of Mercury Electron-Bombardment Ion Thrustors. NASA TN D-4054, 1967.

62. Reader, Paul D.; and Pawlik, Eugene V.: Cathode Durability Tests in Mercury Electron-Bombardment Ion Thrustors. NASA TN D-4055, 1967.

63. Au, Günther F.: Research Work on Electrostatic Ion Propulsion and Electromagnetic Propulsion. Paper 67-724, AIAA, Sept. 1967.

64. Eckhardt, W. O.; Arnold, K. W.; Hagen, G.; Hyman, J., Jr.; Snyder, J.; and Knechtli, R. C.: LM Cathode Electron-Bombardment Thrusters. Paper 67-667, AIAA, Sept. 1967.

65. Masek, Tommy D.; and Womack, James R.: Experimental Studies with a Clustered Ion Engine System. Paper 67-698, AIAA, Sept. 1967.

66. Pawlik, Eugene V.; Nakanishi, Shigeo; and Algeri, Harvey R.: Some Dynamic Characteristics of an Electron-Bombardment Ion Thrustor. NASA TN D-4204, 1967.

67. Banks, Bruce A.; and Richley, Edward A.: Radially Slotted Grids for a Kaufman Ion Thruster. J. Spacecraft Rockets, vol. 4, no. 11, Nov. 1967, pp. 1562-1563.

68. Guman, William J.: Electric Propulsion Activities Outside of the United States. J. Spacecraft Rockets, vol. 4, no. 11, Nov. 1967, pp. 1424-1430.

69. Mickelsen, William R.: Auxiliary and Primary Electric Propulsion, Present and Future. J. Spacecraft Rockets, vol. 4, no. 11, Nov. 1967, pp. 1409-1423.

70. Mickelsen, William R.: Advanced Electric Propulsion Research. Rep. MER-67-68WRM-9, Colorado State Univ. (NASA CR-92560), Dec. 1967.

71. Bechtel, R. T.; Csiky, G. A.; and Byers, D. C.: Performance of a 15-Centimeter Diameter, Hollow-Cathode Thrustor. Paper 68-88, AIAA, Jan. 1968.

72. Staggs, John F.; Gula, William P.; and Kerslake, William R.: Charge-Exchange Ions Downstream of an Ion Thruster. J. Spacecraft Rockets, vol. 5, no. 2, Feb. 1968, pp. 159-164.

73. Nakanishi, S.; Richley, E. A.; and Banks, B. A.: High-Perveance Accelerator Grids for Low-Voltage Kaufman Thrusters. J. Spacecraft Rockets, vol. 5, no. 3, Mar. 1968, pp. 356-358.

74. Masek, T. D.: Plasma Characteristics of the Electron Bombardment Ion Engine. Rep. TR-32-1271, Jet Propulsion Lab., California Inst. Tech. (NASA CR-94554), Apr. 15, 1968.

75. Banks, Bruce: Composite Ion Accelerator Grids. Presented at the Electrochemical Society 3rd International Conference on Electron and Ion Beam Science and Technology, Boston, Mass., May 6-9, 1968.

76. King, H. J.: Mercury Electron-Bombardment Thruster System. J. Spacecraft Rockets, vol. 5, no. 5, May 1968, pp. 591-594.

77. Nakanishi, Shigeo: Experimental Investigation of Mercury Propellant Feed Isolators for Kaufman Thrusters. NASA TM X-1579, 1968.

78. Gallagher, H. E.; and Knauer, W.: Thermionic Cathodes for Kaufman Thrusters. J. Spacecraft Rockets, vol. 5, no. 6, June 1968, pp. 730-732.

79. Lathem, Walter C.: Effects of Electrode Misalinements in Kaufman Thrusters. J. Spacecraft Rockets, vol. 5, no. 6, June 1968, pp. 735-737.

80. Bechtel, Robert T.: Discharge Chamber Optimization of the SERT II Thruster. J. Spacecraft Rockets, vol. 5, no. 7, July 1968, pp. 795-800.

81. LeGrives, E.: French Research on Electric Propulsion: Present Status and Prospects for Development. J. Spacecraft Rockets, vol. 5, no. 7, July 1968, pp. 801-813.

82. Nakanishi, S.; and Pawlik, E. V.: Experimental Investigation of a 1.5-m-diam Kaufman Thruster. J. Spacecraft Rockets, vol. 5, no. 7, July 1968, pp. 801-807.

83. Rawlin, V. K.; and Pawlik, E. V.: A Mercury Plasma-Bridge Neutralizer. J. Spacecraft Rockets, vol. 5, no. 7, July 1968, pp. 814-820.

84. King, H. J.; Molitor, J. H.; and Kami, S.: System Concepts for a Liquid Mercury Cathode Thruster. J. Spacecraft Rockets, vol. 5, no. 8, Aug. 1968, pp. 933-940.

85. Knauer, W.; Poeschel, R. L.; King, H. J.; and Ward, J. W.: Discharge Chamber Studies for Mercury Bombardment Ion Thrusters. Hughes Research Labs. (NASA CR-72440), Sept. 1968.

86. Ward, J. W.; and King, H. J.: Mercury Hollow Cathode Plasma Bridge Neutralizers. J. Spacecraft Rockets, vol. 5, no. 10, Oct. 1968, pp. 1161-1164.

87. Byers, David C.: An Experimental Investigation of a High-Voltage Electron-Bombardment Ion Thruster. J. Electrochem. Soc., vol. 116, no. 1, Jan. 1969, pp. 9-17.

88. Byers, David C.: Effect of Power Supply Impedance on the SERT II Neutralizer. NASA TM X-52543, 1969.

89. Csiky, George A.: Measurements of Some Properties of a Discharge from a Hollow Cathode. NASA TN D-4966, 1969.

90. Byers, David C.: Performance of Various Oxide-Magazine Cathodes in Kaufman Thrusters. NASA TN D-6075, 1969.

91. Cronin, Donald; Goldin, Daniel; and Biess, John: Power Conditioning Suitable for Electric Spacecraft. Paper 69-240, AIAA, Mar. 1969.

92. Csiky, George A.: Langmuir Probe Measurements in a Discharge from a Hollow Cathode. J. Spacecraft Rockets, vol. 7, no. 4, Apr. 1970, pp. 474-475.

93. Day, B. P.; and Fearn, D. G.: A Review of Electric Propulsion Research in the United Kingdom. Paper 69-299, AIAA, Mar. 1969.

94. Goldin, Daniel S.; Lear, Charles W.; and Forrester, A. Theodore: Electron Bombardment Thruster Technology. Paper 69-301, AIAA, Mar. 1969.

95. Hyman, J., Jr.; Bayless, J. R.; Snyder, J. A.; and Eckhardt, W. O.: LM Cathode Electron Bombardment Thrusters. Paper 69-302, AIAA, Mar. 1969.

96. Lazar, James: Review of the NASA Program in Electric Propulsion. Paper 69-248, AIAA, Mar. 1969.

97. Masek, T. D.: Plasma Properties and Performance of Mercury Ion Thrusters. AIAA J., vol. 9, no. 2, Feb. 1971, pp. 205-212.

98. Openshaw, P. R.: Electric Propulsion Systems for European Use. Paper 69-274, AIAA, Mar. 1969.

99. Reader, P. D.; and King, H. J.: Systems Characteristics of Liquid Mercury Cathode Thrusters. Paper 69-237, AIAA, Mar. 1969.

100. Richley, Edward A.; and Kerslake, William R.: Bombardment Thruster Investigations at the Lewis Research Center. J. Spacecraft Rockets, vol. 6, no. 3, Mar. 1969, pp. 289-295.

101. Masek, T. D.; and Pawlik, E. V.: Thrust System Technology for Solar Electric Propulsion. J. Spacecraft Rockets, vol. 6, no. 5, May 1969, pp. 557-564.

102. Banks, Bruce A.: A Fabrication Process for Glass Coated Electron-Bombardment Ion Thruster Grids. NASA TN D-5320, 1969.

103. Cohen, Allan J.: An Electron Bombardment Thruster Operated with a Cusped Magnetic Field. NASA TN D-5448, 1969.

104. Reynolds, Thaine W.; and Richley, Edward A.: Propellant Condensation on Surfaces near an Electric Rocket Exhaust. J. Spacecraft Rockets, vol. 6, no. 10, Oct. 1969, pp. 1155-1161.

105. Lathem, Walter C.: Ion Accelerator Designs for Kaufman Thrusters. J. Spacecraft Rockets, vol. 6, no. 11, Nov. 1969, pp. 1237-1242.

106. Molitor, J. H.; Schwaiger, L.; and MacPherson, D.: Spacecraft Design for Multipurpose Solar Electric Propulsion Missions. J. Spacecraft Rockets, vol. 6, no. 11, Nov. 1969, pp. 1285-1290.

107. Reynolds, Thaine W.; and Richley, Edward A.: Distribution of Neutral Propellant from Electric Thrusters onto Spacecraft Components. NASA TN D-5576, 1969.

108. Bechtel, Robert T.: Performance and Control of a 30-cm-diam, Low-Impulse Kaufman Thruster. J. Spacecraft Rockets, vol. 7, no. 1, Jan. 1970, pp. 21-25.

109. Byers, David C.; and Staggs, John F.: SERT II: Thruster System Ground Testing. J. Spacecraft Rockets, vol. 7, no. 1, Jan. 1970, pp. 7-14.

110. Kerslake, W. R.; Byers, D. C.; and Staggs, J. F.: SERT II: Mission and Experiments. J. Spacecraft Rockets, vol. 7, no. 1, Jan. 1970, pp. 4-6.

111. Milder, Nelson L.; and Sovey, James S.: Preliminary Results of Spectrographic Analyses of Kaufman Thrusters. Paper 70-176, AIAA, Jan. 1970.

112. Poeschel, Robert L.; and Knauer, W.: A Variable Magnetic Baffle for Hollow Cathode Thrusters. Paper 70-175, AIAA, Jan. 1970.

113. Poeschel, R. L.; Ward, J. W.; and Knauer, W.: Study and Optimization of 15-cm Kaufman Thruster Discharges. J. Spacecraft Rockets, vol. 7, no. 1, Jan. 1970, pp. 26-30.

114. Rawlin, Vincent K.; and Kerslake, William R.: SERT II: Durability of the Hollow Cathode and Future Applications of Hollow Cathodes. J. Spacecraft Rockets, vol. 7, no. 1, Jan. 1970, pp. 14-20.

115. Richley, Edward A.; and Reynolds, Thaine W.: Condensation on Spacecraft Surfaces Downstream of a Kaufman Thruster. NASA TM X-52746, 1970.

116. Hall, David F.; Newman, Brian E.; and Womack, James R.: Electrostatic Rocket Exhaust Effects on Solar-Electric Spacecraft Subsystems. J. Spacecraft Rockets, vol. 7, no. 3, Mar. 1970, pp. 305-312.

117. Knauer, W.; Poeschel, R. L.; and Ward, J. W.: Radial Field Kaufman Thruster. J. Spacecraft Rockets, vol. 7, no. 3, Mar. 1970, pp. 248-251.

118. Csiky, George A.: Langmuir Probe Measurements in a Discharge from a Hollow Cathode. J. Spacecraft Rockets, vol. 7, no. 4, Apr. 1970, pp. 474-475.

119. King, H. J.; Poeschel, R. L.; and Ward, J. W.: A 30-cm, Low-Specific-Impulse, Hollow-Cathode, Mercury Thruster. J. Spacecraft Rockets, vol. 7, no. 4, Apr. 1970, pp. 416-421.

120. Lennon, John W.: The Application of a Glass Coating to Electron-Bombardment Ion Thruster Grids by Electrodeposition. Battelle Memorial Inst. (NASA CR-72689), Apr. 1, 1970.

121. Seliger, R. L.; Nudd, G. R.; Grewer, G. R.; and Amboss, K.: Analysis of the Expected Thrust Misalignment of Kaufman Thrusters. J. Spacecraft Rockets, vol. 7, no. 4, Apr. 1970, pp. 422-428.

122. Byers, David C.: Angular Distribution of Kaufman Ion Thruster Beams. NASA TN D-5844, 1970.

123. Masek, T. D.: Plasma Properties and Performance of Mercury Ion Thrusters. Rep. TR-32-1483, Jet Propulsion Lab., California Inst. Tech. (NASA CR-110731), June 15, 1970.

124. Milder, Nelson L.: A Survey and Evaluation of Research on the Discharge Chamber Plasma of Kaufman Thrusters. J. Spacecraft Rockets, vol. 7, no. 6, June 1970, pp. 641-649.

125. Reader, Paul D.; Nakanishi, Shigeo; Lathem, Walter C.; and Banks, Bruce A.: A Submillipound Mercury Electron Bombardment Thruster. J. Spacecraft Rockets, vol. 7, no. 11, Nov. 1970, pp. 1287-1292.

126. Banks, Bruce A.; and Bechtel, Robert T.: 1000-Hour Endurance Test on a Glass-Coated Accelerator Grid on a 15-Centimeter-Diameter Kaufman Thruster. NASA TN D-5891, 1970.

127. Mueller, P. A.; and Pawlik, E. V.: Control Analysis of an Ion Thruster with Programed Thrust. J. Spacecraft Rockets, vol. 7, no. 7, July 1970, pp. 837-842.

128. Bagwell, James W.; Hoffman, Anthony C.; Leser, Robert J.; Reader, Karl F.; Stover, John B.; and Vasiak, Richard W.: Review of SERT II Power Conditioning. Paper 70-1129, AIAA, Aug. 1970.

129. Baumgarth, Siegfried F. J.; Bessling, Harro A. W.; and Sprengel, Uwe W.: Electrostatic Ion Thruster ESKA - 18-P of the DFVLR. J. Spacecraft Rockets, vol. 8, no. 4, Apr. 1971, pp. 305-310.

130. Bechtel, Robert T.: Component Testing of a 30-Centimeter Diameter Electron Bombardment Thruster. Paper 70-1100, AIAA, Aug. 1970.

131. Byers, D. C.; and Snyder, Aaron: Parametric Investigation of Mercury Hollow-Cathode Neutralizers. J. Spacecraft Rockets, vol. 8, no. 2, Feb. 1971, pp. 133-139.

132. Goldin, Daniel S.: Propulsion Module Design for Multimission Solar Electric Spacecraft. Paper 70-1155, AIAA, Aug. 1970.

133. Hall, David F.; and Kelley, L. R.: Experimental Techniques to Determine Electrostatic Rocket Exhaust Effects on Spacecraft Surfaces. Paper 70-1144, AIAA, Aug. 1970.

134. Hyman, J., Jr.; and Bayless, J. R.: Performance of a 20 cm LM Cathode Thruster System. Paper 70-1103, AIAA, Aug. 1970.

135. Jones, Sanford G.; Staskus, John V.; and Byers, David C.: Preliminary Results of SERT II Spacecraft Potential Measurements Using Hot Wire Emissive Probes. Paper 70-1127, AIAA, Aug. 1970.

136. Kaufman, Harold R.; and Vahrenkamp, Richard P.: Some Performance Characteristics of Divergent-Field Bombardment Thrusters. Paper 70-1092, AIAA, Aug. 1970.

137. Kerslake, W. R.; Goldman, R. G.; and Nieberding, W. C.: SERT II - Mission, Thruster Performance, and In-Flight Thrust Measurements. J. Spacecraft Rockets, vol. 8, no. 3, Mar. 1971, pp. 213-224.

138. King, H. J.; and Poeschel, R. L.: A 30 cm Mercury Ion Thruster Module. J. Spacecraft Rockets, vol. 8, no. 4, Apr. 1971, pp. 420-423.

139. Masek, T. D.; and Macie, T. W.: Solar Electric Propulsion System Technology. Paper 70-1153, AIAA, Aug. 1970.

140. Staskus, John V.; and Burns, Robert J.: Deposition of Ion Thruster Effluents on SERT II Spacecraft Surfaces. Paper 70-1128, AIAA, Aug. 1970.

141. Wells, A. A.; Harrison, M. F. A.; and Eden, M. J.: Experimental Studies of Ion Extraction, Ion Loss and Energy Balance in a SERT II Type Ion Thruster. Paper 70-1091, AIAA, Aug. 1970.

142. Speiser, R. C.; and Branson, L. K.: Studies of a Gas Discharge Cesium Ion Source. Paper 2664-62, ARS, Nov. 1962.

143. Sohl, G.; Speiser, R. C.; and Walters, J. A.: Life Testing of Electron-Bombardment Cesium Ion Engines. Paper 66-233, AIAA, Mar. 1966.

144. Sohl, G.; Reid, G. C.; and Speiser, R. C.: Cesium Electron Bombardment Ion Engines. J. Spacecraft Rockets, vol. 3, no. 7, July 1966, pp. 1093-1098.

145. Masek, Tommy D.: Plasma Investigation in a Reversed-Current Electron Bombardment Ion Engine. AIAA J., vol. 5, no. 4, Apr. 1967, pp. 692-698.

146. Sohl, Gordon; Vernon, R. H; Wood, K. G.; and Dillon, T. R.: Performance of a Cesium Bombardment Ion Engine with a Self-Rectifying Discharge and Automatic Controls. J. Spacecraft Rockets, vol. 5, no. 2, Feb. 1968, pp. 165-167.

147. Fosnight, V. V.; Sohl, G.; Goldner, S. J.; and Speiser, R. C.: Cesium Ion Engine System Life Test Results. J. Spacecraft Rockets, vol. 5, no. 4, Apr. 1968, pp. 465-467.

148. Moore, R. D.; Veron, R.; Goldner, S.; and Speiser, R. C.: Cesium Electron Bombardment Thruster Research. Rep. EOS-7240-Final, Electro-Optical Systems, Inc. (NASA CR-98913), Oct. 17, 1968.

149. Sohl, Gordon; and Fosnight, Verryl V.: Thrust Vectoring of Ion Engines. J. Spacecraft Rockets, vol. 6, no. 2, Feb. 1969, pp. 143-147.

150. Fosnight, V. V.; Sohl, G.; Caplinger, E.; Schraut, E. H.; and Dillon, T. R.: A Cesium Electron-Bombardment Microthruster System. Paper 69-293, AIAA, Mar. 1969.

151. Fosnight, V. V.; Dillon, T. R.; and Sohl, G.: Thrust Vectoring of Multiaperture Cesium Electron Bombardment Ion Engines. J. Spacecraft Rockets, vol. 7, no. 3, Mar. 1970, pp. 266-270.

152. Klynn, L. M.; James, E.; Eubanks, A.; and Heslin, T.: Composite Accelerator Electrodes on Cesium Bombardment Thrusters. Paper 70-1089, AIAA, Aug. 1970.

153. Dugan, John V., Jr.: Some Theoretical Bases for Selection of Molecular Ion Propellants and a Survey of Molecular Plasma Collision Processes. NASA TN D-1185, 1964.

154. Byers, David C.; Kerslake, William R.; and Grobman, Jack: Experimental Investigation of Heavy-Molecule Propellants in an Electron-Bombardment Thrustor. NASA TN D-2401, 1964.

155. Milder, Nelson L.: Fragmentation of Anthracene in an Electron-Bombardment Ion Source. NASA TN D-2592, 1965.

156. Reader, Paul D.: The Operation of an Electron-Bombardment Ion Source with Various Gases. Presented at the Electrochemical Society International Conference on Electron and Ion Beam Science and Technology, Toronto, Canada, May 5-7, 1964.

157. Löb, Horst W.: State of the Art and Recent Developments of the Radio Frequency Ion Motors. Paper 69-285, AIAA, Mar. 1969.

158. Bohm, D.: Minimum Ionic Kinetic Energy for a Stable Sheath. The Characteristics of Electrical Discharges in Magnetic Fields. A. Guthrie and R. K. Wakerling, eds., McGraw-Hill Book Co., Inc., 1949, pp. 77-86.

159. Milder, Nelson L.: On the Effects of Monoenergetic Electrons in a Steady-State, Low Pressure Plasma. NASA TN D-6150, 1971.

160. Brode, Robert B.: The Quantitative Study of the Collisions of Electrons with Atoms. Rev. Mod. Phys., vol. 5, no. 4, Oct. 1933, pp. 257-279.

161. Brown, S. C.: Basic Data of Plasma Physics. Technology Press, M.I.T., 1959, pp. 104-105, 114.

162. Spitzer, L., Jr.: Physics of Fully Ionized Gases. Interscience Publ., 1956, pp. 76-81.

163. Dunn, D. A.; and Self, S. A.: Static Theory of Density and Potential Distribution in a Beam-Generated Plasma. J. Appl. Phys., vol. 35, no. 1, Jan. 1964, pp. 113-122.

164. Garscadden, A.; and Emeleus, K. G.: Notes on the Effect of Noise on Langmuir Probe Characteristics. Proc. Phys. Soc. (London), vol. 79, pt. 3, Mar. 1962, pp. 535-541.

NASA-Langley, 1971 — 28 E-6219